



NRL/MR/7130--10-9261

Wide Area Detection and Identification of Underwater UXO Using Structural Acoustic Sensors – 4th Annual Report to SERDP MM-1513

J.A. BUCARO

*Excet, Inc.
Springfield, Virginia*

B.H. HOUSTON

H. SIMPSON

M. SANIGA

A. SARKISSIAN

*Physical Acoustics Branch
Acoustics Division*

D. CALVO

*Acoustic Systems Branch
Acoustics Division*

L. KRAUS

T. YODER

*Global Defense Technology and Systems Inc.
Crofton, Maryland*

July 21, 2010

Approved for public release; distribution is unlimited.

REPORT DOCUMENTATION PAGE				Form Approved OMB No. 0704-0188	
Public reporting burden for this collection of information is estimated to average 1 hour per response, including the time for reviewing instructions, searching existing data sources, gathering and maintaining the data needed, and completing and reviewing this collection of information. Send comments regarding this burden estimate or any other aspect of this collection of information, including suggestions for reducing this burden to Department of Defense, Washington Headquarters Services, Directorate for Information Operations and Reports (0704-0188), 1215 Jefferson Davis Highway, Suite 1204, Arlington, VA 22202-4302. Respondents should be aware that notwithstanding any other provision of law, no person shall be subject to any penalty for failing to comply with a collection of information if it does not display a currently valid OMB control number. PLEASE DO NOT RETURN YOUR FORM TO THE ABOVE ADDRESS.					
1. REPORT DATE (DD-MM-YYYY) 21-07-2010		2. REPORT TYPE Memorandum Report		3. DATES COVERED (From - To) 01 Dec 2008 - 01 Dec 2009	
4. TITLE AND SUBTITLE Wide Area Detection and Identification of Underwater UXO Using Structural Acoustic Sensors — 4th Annual Report to SERDP MM-1513				5a. CONTRACT NUMBER	
				5b. GRANT NUMBER	
				5c. PROGRAM ELEMENT NUMBER 63716D8Z	
6. AUTHOR(S) J.A. Bucaro,* B.H. Houston, H. Simpson, D. Calvo, L. Kraus,† T. Yoder,† M. Saniga, and A. Sarkissian				5d. PROJECT NUMBER MM-1513	
				5e. TASK NUMBER	
				5f. WORK UNIT NUMBER 71-9024	
7. PERFORMING ORGANIZATION NAME(S) AND ADDRESS(ES) Naval Research Laboratory, Code 7130 4555 Overlook Avenue, SW Washington, DC 20375-5320				8. PERFORMING ORGANIZATION REPORT NUMBER NRL/MR/7130--10-9261	
9. SPONSORING / MONITORING AGENCY NAME(S) AND ADDRESS(ES) SERDP Program Office 901 North Stuart St., Suite 303 Arlington, VA 22203				10. SPONSOR / MONITOR'S ACRONYM(S) SERDP	
				11. SPONSOR / MONITOR'S REPORT NUMBER(S)	
12. DISTRIBUTION / AVAILABILITY STATEMENT Approved for public release; distribution is unlimited.					
13. SUPPLEMENTARY NOTES *On-site contractor with Excet, Inc. Springfield, Virginia 22151 †On-site contractor with Global Defense Technology & Systems, Inc. Crofton, MD 21114					
14. ABSTRACT This project is exploring the development of a structural acoustics (SA) based sonar methodology for wide area search and identification of underwater unexploded ordnance (UXO). This approach has significant advantages over conventional acoustic approaches relying on formation of high resolution images including: diverse set of “fingerprints” leading to low false alarm rates; longer range leading to wide area coverage; and low frequency sediment penetration leading to buried target prosecution. A core element of the project is an examination of the scattering features exhibited by typical UXO targets in the SA regime using NRL's state-of-the-art underwater scattering facilities, both laboratory-based and at-sea. We have extended the original mono-static data base to include bi-static data from proud and partially buried targets, examined the special case of forward scattering and how it might be exploited, connected laboratory UXO scattering measurements to those made in St. Andrew's Bay by employing an advanced acoustic multi-path propagation model, and examined the scattering from proud and buried targets on smooth and rough sediment surfaces using an elasto-dynamic finite integration technique (EFIT) numerical simulation model.					
15. SUBJECT TERMS Structural Acoustic Sensors UXO Detection/Identification					
16. SECURITY CLASSIFICATION OF:			17. LIMITATION OF ABSTRACT SAR	18. NUMBER OF PAGES 40	19a. NAME OF RESPONSIBLE PERSON B.H. Houston
a. REPORT Unclassified	b. ABSTRACT Unclassified	c. THIS PAGE Unclassified			19b. TELEPHONE NUMBER (include area code) (202) 404-3840

CONTENTS

LIST OF ACRONYMS

CSS – Coastal System Station
EFIT – Elasto-dynamic finite integration technique
KMP – Kernel matching pursuits
LDV – Laser Doppler vibrometry
LSA – Laboratory for Structural Acoustics
NAH – Nearfield acoustic holography
NRL – Naval Research Laboratory
PE – Parabolic Equation
PML – Perfectly matched layer
RAM – Range dependent acoustic model
RVM – Relevance vector machine
SA – Structural acoustic
SONAR – Sound navigation & ranging
TS – Target Strength
UXO – Unexploded ordnance

LIST OF FIGURES

Figure 1 — Structural acoustic ID vs. imaging

Figure 2 — NRL laboratory for Structural Acoustics. One million gallon pool facility with adiabatic walls and acoustic coatings, vibration isolation system, and complex acoustic scanners, sources, and processing algorithms.

Figure 3 — Experimental measurement geometry. The target is placed in the plane-wave region of (1) a near-field cylindrical source at low frequency (LF) or (2) a farfield piston source at high frequency (HF) with a nearly co-located broadband short vertical receiver array. The target (which is ~ 2.7 m from the receiver) is rotated over a full 360 degrees in increments of 1 degree.

Figure 4 — a) The three UXO sonar source/receiver configurations. b) Range of conditions associated with a target search.

Figure 5 — a) Broadside target strength versus frequency computed for infinite cylindrical shell with five inch rocket parameters and 3D wave correction compared to measurement. Black: measured data; red: COMSOL 2D FE calculation with 3D wave correction; green-dashed: $10\log_{10}(aL^2/2\lambda)$; green-dashed-dot: wave theory rigid 2D cylinder with finite length 3D wave theory correction. b) Comparison Between the EFIT and finite element broadside scattering predictions for infinite cylindrical shell with five inch rocket parameters and 3d wave correction. Target strength in dB: red – EFIT; black- finite element both wave-corrected for 3D.

Figure 6 — Scattering geometry for EFIT calculations

Figure 7 — a) EFIT model result for infinite cylindrical shell with five inch rocket parameters and 3D wave correction compared to laboratory measurement for free-field five-inch rocket target. b) EFIT model result for proud infinite cylindrical shell with five inch rocket parameters and 3D wave correction compared to laboratory measurement for proud five-inch rocket target. c) EFIT model result for half-buried infinite cylindrical shell with five inch rocket parameters and 3D wave correction compared to laboratory measurement for half-buried five-inch rocket target.

Figure 8. — Backscattered target strength versus frequency calculated using EFIT model for infinite cylindrical shell with five inch rocket parameters and 3D wave correction for geometry shown in Fig. 6 and various burial conditions.

Figure 9. — Example surface roughness realizations

Figure 10 — a) Target strength versus frequency and receiver angle. Effects of roughness for flush-buried infinite cylinder target with sound incident at beam on the target and 2 degrees with respect to the sediment surface. b) Target strength versus frequency and receiver angle. Effects of roughness for flush-buried infinite cylinder target with sound incident at beam on the target and 90 degrees with respect to the sediment surface.

Figure 11. — Ensemble averaged reverberation backscattered intensity. Time series for the half-buried infinite cylinder and a 2 degree source angle.

Figure 12. — Ensemble averaged target echo versus reverberation backscattered intensity. The time series are shown for 2°, 28° (critical angle), and 90° source angles. The simulation used a wide-band Ricker source pulse centered at 10 kHz covering a band 2 kHz to 30 kHz.

Figure 13. — Bistatic TS measurements for five-inch rocket. Bistatic target strength displayed in dB as a color map measured for the five-inch rocket.

Figure 14. — Measured forward scattering TS versus analytic model. Measured free-field forward scattered target strength versus frequency in black. (a) 90° source; blue/green soft/rigid boundary condition theory, respectively; (b) 0° source; blue theory.

Figure 15. — Possible forward scattering system geometry, corresponding range-cross range plots, and forward scattered ts versus frequency and angle. (a) Hypothetical long range forward scattering measurement range: R_{ST} , R_{SR} , and R_{TR} are the source to target distance, the distance from the source to a particular receiver, and the distance from the target to a particular receiver, respectively; (b) time-cross range plots in dB for the direct source 150 meters from the center receiver (heavy line) and for the forward scattered signal $\times 30$ with TS given by Eq. 4; (c) scattering TS in dB versus frequency and angle in the forward scattered sector for the scattering response given by Eq. (4); and (d) that extracted from the numerical results shown in (b).

Figure 16. — Measurement details at St. Andrew's Bay. Upper right: Measurement site and water depths; lower right: UXO targets and their positions and the locations of the source and rail based sensor system; upper left: drawing of the source and rail system with both a moving source and receiver.

Figure 17. — Measured target strength. Magnitude of the bistatic target strength for 0° incidence coded in color versus frequency and scattering angle as measured in the Bay (left) and in the sediment pool (right) for the proud 155 mm shell.

Figure 18. — Measured target strength. Magnitude of the bistatic target strength for 0° incidence coded in color map versus frequency and scattering angle as measured in the Bay (left) and in the sediment pool (right) for the proud 155 mm shell.

Figure 19. — Simulated effect of propagation on the monostatic TS. Upper left: Measured monostatic free-field target strength versus angle and frequency for the 155 mm shell shown in the upper photograph; lower: the measured and simulated (using RAM) acoustic pressure in the water and sediment versus time at the receiver for the St. Andrew's Bay site.

Figure 20. — The major rays which account for the acoustic propagation in the water column and sediment. Upper: The important rays from the source to the receiver array; lower: the measured and simulated (using RAM) acoustic pressure in the water and sediment versus time at the receiver for the St. Andrew's Bay site with some of the ray arrival times identified with arrows.

Figure 21. — Target strength versus frequency and aspect measured in St. Andrew's Bay compared to that simulated using RAM and the laboratory measured free-field TS. In the bay results, the stationary source and moving receiver are 42 and 52 meters, respectively, from the 155 mm shell target.

EXECUTIVE SUMMARY

This document represents the fourth annual report for the SERDP sponsored scientific effort at the Naval Research Laboratory involving structural acoustic-based detection and identification of underwater unexploded ordnance (UXO). The report covers work performed during the period December 1, 2008 through December 1, 2009.

Many active and former military installations have ordnance ranges and training areas with adjacent water environments in which UXO now exists due to wartime activities, dumping, and accidents. These contaminated areas include coastal and inland waters both in the United States and abroad. SERDP goals require the development of innovative technologies able to separate UXO from false targets and to discriminate amongst individual UXO targets themselves. Over time, such geographic areas are becoming less and less remote as the adjacent lands become further developed, and the potential hazard to the public from encounters with such UXO has begun to rise. Presently there exists no sufficiently effective capability to survey such underwater areas and map UXO locations.

This project is exploring the potential for developing a structural acoustics (SA) based sonar methodology for wide area search and identification of UXO. This new approach may have significant advantages over more conventional acoustic approaches which rely on the formation of high resolution images.

Conventional sonar approaches which form images must operate at relatively high frequencies since the image resolution cell size is directly proportional to the acoustic wavelength. In this regime, acoustic wavelengths are short compared to the target dimensions and the waves are scattered for the most part from the external boundary of the target (specular scattering). In contrast, in the structural acoustic regime, acoustic wavelengths are comparable to, or longer than, the target dimensions. Sound readily penetrates the target, and the acoustic scattering is now related to the vibrational dynamics of the object, both whole-body and internal structure. The time-frequency features in the scattered echoes can then be used to “fingerprint” the target without the need to form an image.

The inherent advantages of the SA approach include: diverse set of “fingerprints” leading to low false alarm rates; longer range operation leading to wide area coverage; and low frequency sediment penetration leading to buried target prosecution.

The program is structured to answer three fundamental questions about UXO structural acoustic scattering phenomenology in a marine environment. 1) Does enough acoustic energy reach proud/buried UXO to produce a detectable and exploitable scattered signal? 2) Are the structural-acoustic signatures and the features derived there-from of underwater UXO and clutter sufficiently separable in a marine environment? 3) Can we structure identification algorithms so as to be robust with respect to the environmental and historical circumstances? We believe successful prosecution of the program tasks will answer these questions in the affirmative and provide the foundation for a new structural acoustics-based approach for identifying proud and buried UXO objects.

The four main tasks include: 1) experimental measurements of the structural acoustic UXO and false target responses; 2) demonstration of the ability to separate UXO and false targets using structural acoustic features; 3) the development of robust identification algorithms which could exploit the

structural acoustic features regardless of the environment or historical conditions; and 4) prosecution of a test program both in the laboratory free-field and sediment facilities and in the waters off Panama City Florida for the purpose of more fully characterizing targets and clutter as they would present themselves in real-world environments. The focus of the effort is to understand what features are important for determining whether detections in a real-world environment are or are not associated with UXO. Understanding the basic underwater scattering phenomenology for UXO and clutter in the structural acoustics band and then determining the environmental impact on the scattering phenomenology is the key to generating features that will provide robust target detection and identification in the real-world applications of this technology.

In the first two years of the program, we completed comprehensive acoustic scattering measurements in the free field on a number of actual UXO's over a broadband of frequencies which include the structural acoustics domain. The 6 targets include an 80 mm mortar round, a 120 mm mortar round, a 155 mm artillery shell, a 5 inch rocket warhead, each filled with a material system designed by NRL to approximate the elastic moduli and density of generic materials typically found in these devices, a 25 mm M794 dummy cartridge whose cavity is filled with an epoxy resin to approximate the weight of service cartridges and a 105 mm solid sabot practice round. These measurements were carried out in the NRL Laboratory for Structural Acoustics, a state-of-the-art, heavily instrumented, 17 m diameter by 15 m deep pool facility covering the frequency band from 1 kHz to 140 kHz. Monostatic measurements (co-located source and receiver) were made in the free-field over a full 360 degrees and at 1 degree angle increments. To our knowledge, these data sets represent the first of their kind for actual UXO targets. Several important conclusions can be drawn upon observation of the data. (1) In general, there are a number of angular aspects that provide relatively high target strength levels (~ -10 dB to -20 dB). Based upon our experience, this implies that these targets, even though relatively small, would be detectable in this structural acoustics band out to long ranges (10's to 100's of meters) in most acoustic environments. (2) The associated features appear to be exploitable for target identification. For example, the scattering features are clearly separable from those we have seen from non-UXO targets. Our results also indicate that the data will support feature-based separation of various classes of UXO. The various structural acoustic mechanisms that lead to exploitable features include for example whole body and interior structure resonances, ring resonances, and a number of specular highlights. (3) As expected, the measured scattering patterns from all six targets have almost perfect right/left symmetry, and we believe this can also be exploited for separating such UXO from most natural irregularly shaped objects. We also made similar measurements over this frequency band for four non-UXO targets including a large rock and a cinder block and for two concrete-filled metal pipes. These are used as "false targets" in our studies to determine the ability of our identification algorithms to separate the UXO from the false targets. The latter are also "overlap targets" whose scattering has been measured by CSS Panama City thus allowing a controlled comparison between the findings of the two groups. The structural acoustic data bases were processed using feature extractors such as matching pursuits, and this led to a positive result for the first critical "go-no go" decision point in the second year. At this point the ability to separate UXO and false targets based on their structural acoustic features has been demonstrated using the data collected in the laboratory facilities. In some cases structural acoustic features could be integrated with responses from SERDP near-range sensors such as induction detectors in order to further increase identification performance. To permit evaluation of this possibility at a later time, inductive measurements were also carried out in the NRL pool facility using a Geonics Limited EM61-MK2 submersible induction sensor system on the 155 mm artillery shell filled with the simulant material. The completed data base will be used at a future time to evaluate the merits associated with combining structural acoustic ID with this additional sensor modality.

Measurements of the scattering from some of the UXO targets in the NRL sediment bottom facility, initiated at the end of the second year, were completed in the third year. The targets included the 155 mm shell and the five inch rocket warhead. Measurements in this facility included monostatic

scattering signatures from these two targets placed proud of the sediment over the band of frequencies 2 kHz to 30 kHz. These measurements were compared to monostatic measurements made in the free-field, and this indicated that presence of the sediment did not produce significant changes in the general frequency/angle responses patterns. However, the levels of some features were affected, and for the most part (but not always) resulted in scattering increases. That the target scattering levels are maintained (and to some extent even increased) implies that for the proud case neither does backscattering from the sediment overwhelm the target scattering nor do sediment effects alter the target scattering mechanisms. Indeed, the UXO on the sediment remains very detectable in the structural acoustics band. That the frequency/angle characteristics have not been significantly altered by the presence of the sediment and its boundary implies that feature-based identification algorithms trained on pool data ought to be robust when applied to the same target found proud on a similar sediment. This is a significant step forward for our methodology which up to now has been demonstrated only with and on free-field targets.

We expanded the data base for these two targets to the bistatic case wherein the source and receiver could be at different positions (angles). These measurements were again made with the target proud of the pool sediment, and they included two angles of incidence, 0° (source at the front of the target) and 90° (source at the beam of the target). These measurements included both the backscattered plane and the forward scattered plane. Regarding the proud measurements, we make the following two observations which can be taken as general only to the extent that we have captured the salient behavior of the bistatic mechanisms by sampling just two source angles (0° and 90°). First, given the rough agreement between the predicted backscattering levels which do not take into account the sediment (especially recognizing the deviation of these targets from a perfect cylinder), for the proud targets the effect of the sediment on TS is not large. Except for the backscattered return from the anomalous front of the 155 mm shell, this is consistent with other results we have obtained comparing free-field and proud cases for monostatic scattering. Second, we see the largest target strength by far in the bistatic case and for the forward scattered echo. Further, this feature exists over nearly the entire band.

We concluded from this limited study that access to bistatic echo information in operations aimed at detecting submerged UXO targets could provide an important capability. If the high forward scattered levels persist upon burial, bistatics could be especially important for buried targets being prosecuted by sonars operating over smooth bottoms below the critical angle in order to achieve some range.

Research in the fourth year, focused on the collection of laboratory-grade data sets regarding target burial and vertical orientation, the analysis of these data bases employing advanced multi-path, sediment-based numerical structural acoustic models, and the determination of the impact of these effects on scattering and on the associated structural acoustic features.

First, we considered the largest target strength levels which are associated with the forward scattered echo. Obtaining an exploitable forward scattered echo is considerably more difficult than doing so for back-scattered signals because of the simultaneous presence of the strong incident field. We overcame this difficulty in our laboratory measurements in a straightforward manner because we were able to map the details of the incident field with high precision before placing the target into position. Clearly, this is not possible in a search for UXO targets in the environment. However, the high forward scatter target strength levels which persist even upon burial warrant consideration of how this might be accomplished. One possibility which we explored is based on the following considerations. (1) There is an angular region (here beyond $\sim \pm 20^\circ$ from forward) with no overlap of source and echo time signals, and here the forward scattered component is directly accessible. (2) In the overlap region, we would like to subtract the “known” source signal at each receiver from the total signal using the appropriate Green’s function leaving the desired scattered pressure. However, the source signal is not known precisely due to the unknown random deviations of the receiver locations. We can, however, estimate each receiver position deviation by finding the local minimum for the difference between the received signal (the sum

of the source, scattered, and noise signals) and an estimate of the source signal based on the known Green's function. Good estimates of the receiver deviations are so obtained because the source signal is much stronger than the other components of the received signal. We successfully demonstrated this approach numerically.

We also carried out numerical studies of backscattering from the 5" rocket UXO near a smooth or rough water-sand interface using EFIT two-dimensional simulation model. The elastodynamic finite integration technique (EFIT) code is a time-domain method which uses a time-domain version of a perfectly matched layer (PML) to truncate boundaries. The code is useful for the treatment of pulse propagation in inhomogeneous fluid-elastic environments such as are of interest in the underwater UXO problem. The generality of EFIT allows for the inclusion of stratified bottoms with rough interfaces and volume inhomogeneities such as rocks, shells, and other buried objects. Using EFIT, we studied the below critical angle backscattering from the beam of an infinitely long cylindrical target for the free-field, proud, half-buried and flush buried target cases. We also studied the effect of a random rough sediment surface both on the target scattering and from the sediment-water interface itself. The following conclusions can be drawn from these studies. (1) For a proud target, the impact of the surface of a smooth sediment is minimal compared to the free-field case. In particular, at some frequencies the sediment acts to increase the target strength while at others to decrease it. However, in both cases the changes are relatively small. (2) Burial causes a large decrease in the target strength. Except at the lowest frequencies, even only half burial results in roughly a 10 dB decrease. In the flush burial case, however, there is anywhere from a 15 to 25 dB decrease across the band. (3) At grazing angles (and thus for the more long range configurations), the reverberant background level is only moderately increased. However, there are some probably important changes in the frequency-angle feature structure. At look-down angles, there is a relatively larger increase in the background reverberant level. But there is less change in the frequency-angle structure. (4) In the time window of the scattered target response, the reverberation from the rough sediment boundary generally increases as the source angle grows, from grazing conditions at the smallest angle to 90 degrees (having the sound source vertically above the target), and this is not surprising.

In the previous year, scattering measurements were carried out on several proud UXO targets in St. Andrew's Bay where the water depths were on the order of 30 feet. This past year, the data associated with one of the targets, the 155 mm shell, was analyzed with reference to measurements made in the sediment pool facility at much shorter ranges. The objective was to understand the differences observed for target scattering in these two environments. The differences observed between the very short range sediment pool measurements and the measurements in the bay are most likely due to one or more of the following conditions: (1) sediment properties; (2) geometric uncertainties; and (3) acoustic propagation. We believe that the largest effect by far relates to the last item, and we have considered this effect in some detail.

In particular, we have used the Range-dependent Acoustic Model (RAM) model developed at NRL by Michael Collins. This model is based on a user-selected multiple-term Padé approximation of the parabolic equation (PE) operator. Because this solution allows range steps much greater than the acoustic wavelength and does not require fine vertical gridding, RAM is a very fast research model. Having demonstrated the use of the RAM code and the effects of multi-path propagation, we then attempted to relate the measured target strength for the 155 mm shell made in the laboratory at short range (2 meters) and which contains only direct path rays to that measured in St Andrew's Bay at a range of 42 m and having significant multi-path propagation. Specifically, we used the RAM code and the free-field measured target strength to predict what would be measured in the Bay. The introduction of the effects of multi-path propagation go a long way in producing the frequency-angle patterns actually measured at the longer ranges in the Bay. The remaining differences could be related to several factors. First, the sediment surface, assumed in our RAM projection to be flat, is actually not perfectly so. Second, there is some uncertainty regarding positioning of the target orientation and the source alignment.

The fifth year of the program will focus on the collection of additional at-sea data bases in the structural acoustics frequency band at the Panama City off-shore site together with measurements in the sediment pool facility. The objective here is to more fully characterize targets and clutter as they would present themselves in real-world environments. The focus of the effort will be to understand what features are important for determining whether detections in a real-world environment are or are not associated with a UXO.

OBJECTIVE

The objective for SERDP Project MM-1513 is to address the technical issues necessary to implement an innovative structural-acoustics (non-imaging) sonar system for wide search area identification using structural acoustic features from proud and buried UXO objects. In addition to providing wide-area capability, the structural-acoustic features are also effective at shorter ranges and may be integrated with other SERDP near-range sensors including magnetometer, induction, and acoustic-imaging devices to increase identification performance. In contrast to imaging, the structural-acoustic technique exploits both non-specular and specular scattering features. This represents a new approach to acoustic identification of UXO; and we believe a number of exploitable structural-acoustic mechanisms exist for the in-water UXO problem and that the features derived there-from will be sufficiently separable from individual classes of UXO and from those associated with clutter. Further, some of the features should manifest themselves at frequencies where significant bottom penetration persists, allowing detection and identification of buried UXO not only for shorter range, down-looking sonars but at longer ranges as well.

The broad objective stated above can be broken into four goals. The first is to understand the UXO target and clutter structural acoustic scattering signature phenomenology by performing controlled, high fidelity acoustic scattering measurements in the laboratory facilities. This objective was met in the first year of the program through laboratory measurements on target set 1, and the effort was extended to target set 2 in the second year. The second goal is to extract structural-acoustic features from scattered echoes collected in the laboratory and to demonstrate that UXO and clutter can be separated via kernel-based identification algorithms exploiting these features. This goal was achieved in the second year as it relates to laboratory data and is now being pursued regarding at-sea data. The third goal is to apply active-learning paradigms such as concept drift developed under previous SERDP support and determine the extent to which various techniques might allow structural acoustic identification techniques trained on laboratory data free-field data to be effective when used in the presence of a sediment and ultimately in the real environment. The first part of this goal was addressed in the third year of the program. The fourth goal upon which the 2009 and 2010 effort is focused is to carry out a test program both in the laboratory free-field and sediment facilities and in the waters off Panama City Florida for the purpose of more fully characterizing targets and clutter as they would present themselves in real-world environments. The focus of the effort is to understand what features are important for determining whether detections in a real-world environment are or are not associated with UXO. Understanding the environmental impact on the scattering phenomenology as understood through laboratory grade experiments conducted in the real environment together with comparisons to the predictions from advanced the multi-path, sediment-based numerical structural acoustic models is the key to being able to exploit scattering features that will provide robust target detection and identification in non-laboratory, real-world scenarios.

BACKGROUND

Many active and former military installations have ordnance ranges and training areas with adjacent water environments in which UXO now exists due to wartime activities, dumping, and accidents. These contaminated areas include coastal and inland waters both in the United States and abroad. SERDP

goals require the development of innovative technologies able to separate UXO from false targets and to discriminate amongst individual UXO targets themselves. Over time, such geographic areas are becoming less and less remote as the adjacent lands become further developed, and the potential hazard to the public from encounters with such UXO has begun to rise. Presently there exists no sufficiently effective capability to survey such underwater areas and map UXO locations.

This project (SERDP Project MM-1513) is exploring the potential for developing a structural acoustics (SA) based sonar methodology¹ for wide area search and identification of underwater unexploded ordnance (UXO). This new approach may have significant advantages over more conventional acoustic approaches which rely on the formation of high resolution images. These advantages include: diverse set of “fingerprints” leading to low false alarm rates; longer range operation leading to wide area coverage; and lower frequency sediment penetration leading to buried target prosecution².

Conventional sonar approaches which form images (see Fig. 1) must operate at relatively high frequencies since the image resolution size is directly proportional to the acoustic wavelength. In this regime, acoustic wavelengths are short compared to the target dimensions and the waves are scattered for the most part from the external boundary of the target (specular scattering). In contrast, in the structural acoustic regime, acoustic wavelengths are comparable to, or longer than, the target dimensions. Sound readily penetrates the target, and the acoustic scattering is now related to the vibrational dynamics of the object, both whole-body and internal structure. The time-frequency features^{3,4} in the scattered echoes can then be used to “fingerprint” the target without the need to form an image.

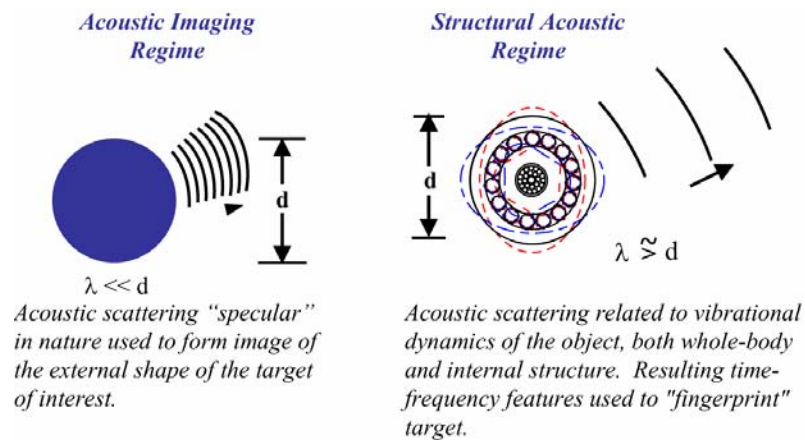


Figure 1 – Structural Acoustic ID vs. Imaging

MATERIALS AND METHODS

The tasks described below answer three fundamental questions about UXO structural acoustic scattering phenomenology in a marine environment. 1) Does enough acoustic energy reach proud/buried UXO to produce a detectable and exploitable scattered signal at reasonable ranges? 2) Are the structural-acoustics signatures from underwater UXO and clutter sufficiently separable in a marine environment? 3) Can we structure identification algorithms so as to be robust with respect to the environmental and historical circumstances? We believe successful prosecution of the program tasks will answer these questions in the affirmative and provide the foundation for a new structural acoustics-based approach for identifying proud and buried UXO objects. The four main tasks include: 1) experimental measurements of the structural acoustic UXO and false target responses; 2) demonstration of the separability of UXO and false targets using structural acoustic features; 3) the development of robust identification algorithms

which could exploit the structural acoustic features regardless of the environment or historical conditions; and 4) prosecution of a test program both in the laboratory free-field and sediment facilities and in the waters off Panama City, Florida, for the purpose of more fully characterizing targets and clutter as they would present themselves in real-world environments. The focus of the effort is to understand what features are important for determining whether detections in a real-world environment are or are not associated with UXO. Understanding the basic underwater scattering phenomenology for UXO and clutter in the structural acoustics band and then determining the environmental impact on the scattering phenomenology is the key to generating features that will provide robust target detection and identification in the real-world applications of this technology.

A core element of the current project is a comprehensive examination of the scattering levels and features exhibited by typical UXO targets in the SA regime using NRL's state-of-the-art underwater scattering facilities, both laboratory-based⁵ and at-sea⁶.

In the first year⁷, a representative UXO target set (target set 1) was identified, and the specific targets obtained from the Aberdeen Proving Grounds. This four target set included a 155 mm artillery shell, a 5 inch rocket warhead, an 80 mm mortar round, and a 120 mm mortar round. Each target was then filled with a material system designed by NRL to roughly approximate the elastic moduli and density of material typically found in these devices. In the second year, additional targets were added to this UXO list. These included a 105 mm sabot solid projectile, a water-flooded 120 mm mortar round, a 25 mm M794 dummy cartridge whose cavity is filled with an epoxy resin to approximate the weight of service cartridges, and two so-called overlap targets to be used both as false targets and in comparisons of the measurements made at NRL to those made at the Coastal Systems Station Laboratory (CSS) in Panama City, Florida. The overlap targets were two different size concrete-filled metal pipes. In addition to the UXO targets, a large rock and a common cinder block were used to represent further examples of potential false targets.

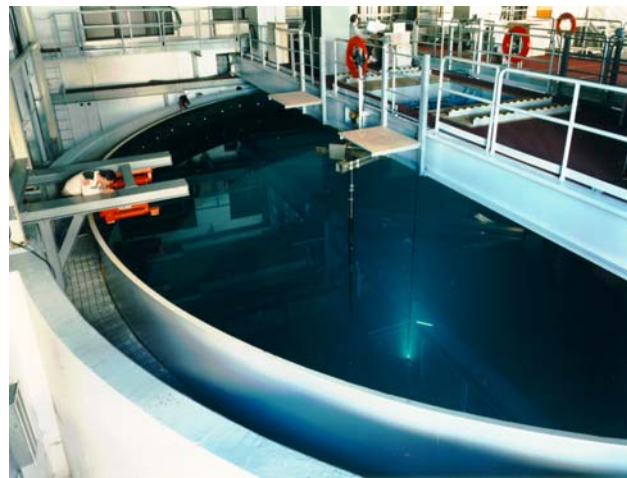


Figure 2 – NRL Laboratory for Structural Acoustics One million gallon pool facility with adiabatic walls and acoustic coatings, vibration isolation system, and complex acoustic scanners, sources, and processing algorithms.

Systematic free-field acoustic scattering measurements were carried out in the NRL Laboratory for Structural Acoustics Facility (Fig. 2) yielding full 360 degree broadband (1 kHz - 140 kHz) data bases. These measurements were completed on target set 1 in 2006, and in 2007 the broadband measurements were extended to the 105 mm sabot solid projectile, the 25 mm solid dummy round, the two overlap targets, and the large rock and the common cinder block false targets. These measurements⁸ made in the free-field were then augmented by those made on some of the targets proud of the bottom using a companion sediment scattering facility and an at-sea rail-based system in St. Andrew's Bay, Florida. The Laboratory for Structural Acoustics (LSA)⁵ at NRL (see Fig. 2) is a state-of-the-art underwater acoustic research laboratory unique in the world. The LSA infrastructure includes a large cylindrical one million gallon (17 m diameter \times 15 m deep) de-ionized water tank located in Building 5. This tank is vibration isolated, temperature controlled, and heavily instrumented with in-water precision robots for nearfield acoustic holography (NAH), laser Doppler vibrometry (LDV), and compact range measurements. The free-field scattering measurements were conducted with the facility in its compact scattering range mode as shown in Fig. 3. Each UXO target was suspended at mid-depth in the tank

together with the source and receiver. Two sources were used for these experiments. The first source is a 3 meter long nearfield line array mounted horizontally. The array elements are shaded in such a way as to produce a plane-wave sound field in its nearfield throughout a limited volume centered at the target position. The line array generates a broadband pulse approximately 2 μ s in duration and covers the band from 1 – 25 kHz. The receiver used in these experiments is a vertical line array that was also suspended at the mid-depth of the tank. A second piston-like source was used to collect data in the band from 8 kHz – 140 kHz. The measurement system is designed for collection of both monostatic and bistatic scattering data. For the measurements made in the first two years, only the monostatic configuration was used, i.e. the source and receiver fall along the same bisector to the target center. The scattered echo response was measured 2.7 meters from the target in 1 degree increments over 360 degrees. The data was processed to recover full complex scattering cross-sections expressible as target strength referenced to 1 meter in the following way. In order to obtain the target strength, three quantities are measured: the incident acoustic pressure, the pool clutter (background) pressure, and the scattered pressure. First, the source is excited and the incident pressure measured at the location corresponding to the target center for the scattering measurement. Second the source is excited and the clutter pressure field measured at the location at which the receiver will be placed for the scattering experiment. Lastly, the target is inserted and the scattered pressure field measured.

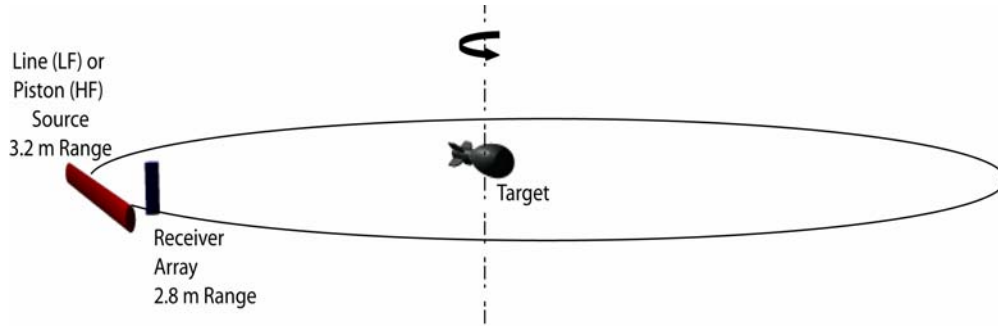


Figure 3 – Experimental Measurement Geometry

The target is placed in the plane-wave region of (1) a near-field cylindrical source at low frequency (LF) or (2) a farfield piston source at high frequency (HF) with a nearly co-located broadband short vertical receiver array. The target (which is ~ 2.7 m from the receiver) is rotated over a full 360 degrees in increments of 1 degree.

In this method, the time domain scattered data from the target at a given aspect angle is cleaned to remove unwanted reflections (clutter) not associated with a target return, Fourier transformed, and then normalized by a reference measurement. The target strength is obtained by first subtracting the clutter measurement from the scattering measurement. This process removes energy from any indirect paths due to reflections from the finite - sized pool boundaries or submerged equipment. This step is only possible through precise control of the locations of the acoustic elements and only if fluctuations in the acoustic medium are sufficiently small. For our facility (which meets these demands), robotic control of the source and receiver position is approximately 30 microns, and the iso-velocity water is maintained to within 0.01° C for more than a 24 hour period. With the clutter removed from the scattered signal, the parameter $X(f, \theta)$ is formed in terms of the scattered signal, $P_{scat}(f, \theta)$, and the incident field measured at the target center, $P_{inc}(f)$:

$$X(f, \theta) = \frac{P_{scat}(f, \theta)}{P_{inc}(f)} \frac{r_{scat}}{e^{ikr_{scat}}}, \quad (1)$$

where r_{scat} is the distance from the target center to the receiver. The target strength⁹ (TS) is then defined and displayed as $10\log_{10}(|X(f,\theta)|^2)$. The basic data acquisition parameters are summarized as follows: overall bandwidth 1 kHz – 140 kHz; sample rate (per channel) 500 kHz (min.); record length (per channel) ~32 k; record length (time) 16 ms; ensemble number ~16; dynamic range ~ 80 dB; and typical measurement duration ~1 week.

It is anticipated that in some cases structural acoustic features could be integrated with responses from existing SERDP near-range sensors such as induction detectors in order to further increase identification performance. To permit evaluation of this possibility at a later time, inductive measurements were also carried out using a Geonics Limited EM61-MK2 submersible sensor system, a high powered time domain pulsed-induction device suitable for detecting both ferrous and non-ferrous metals. Metallic objects interact with the transmitted field inducing secondary fields which are subsequently detected by coils co-located with the transmitter. The data was collected on a battery operated data acquisition system which was also provided by Geonics and down-loaded to a PC. In these measurements, the 155 mm artillery shell target filled with the epoxy filler was hung with Kevlar fishing line (non-magnetic) in the NRL pool facility. The measurements, taken as ensemble data to be averaged off line, were monostatic covering angular aspects from 0 to 360 in increments of 15 degrees with a source/receiver to target center distance of 1.27 m. The completed data base will be used at a future time to evaluate the merits associated with combining structural acoustic ID with this additional sensor modality.

In the second year¹⁰, the target set 1 and target set 2 data bases were processed using feature extractors such as matching pursuits, and this led to a positive result for the first critical “go-no go” decision point in the second year. Kernel-based algorithms such as Relevance Vector Machines¹¹ (RVM) and Kernel Matching Pursuits¹² (KMP) which use the structural acoustic features for identification were demonstrated using the experimental data bases. Measurements in the sediment pool facility begun in the second year were continued into the third year. Also in the third year, targets were seeded in the maritime environment off the coast of Panama City, and acoustic scattering data were collected using an existing rail-based measurement system. In order to allow the structural acoustic identification algorithms to adapt to new site-specific details such as target type/orientation and environmental conditions, the development of a concept drift active learning identification algorithm suitable for UXO was initiated in the second year, and the plan was to test it in the third year off-line using all the data collected in the previous tasks¹³. Research in the fourth year, focuses on the collection of laboratory-grade data sets regarding target burial and vertical orientation, the analysis of these data bases employing advanced multi-path, sediment-based numerical structural acoustic models, and the determination of the impact of these effects on scattering and on the associated structural acoustic features. The fifth year focuses on the collection of additional at-sea data bases in the structural acoustics frequency band at the Panama City off-shore site. The objective here is to more fully characterizing targets and clutter as they would present themselves in real-world environments. The focus of the effort will be to understand what features are important for determining whether detections in a real-world environment are or are not associated with a UXO.

This program has successfully demonstrated that typical UXO scatter appreciable levels of sound over what we call the structural acoustics domain, that these signals would be detectable at modest ranges in most environments of interest, and that in the free-field case structural acoustic features can be used to separate UXO from other targets. The efforts in this program are now seeking to fill in the scientific and engineering gaps necessary to allow the demonstration of UXO sonars based on the structural acoustic ID paradigm. The related issues are being addressed in the context of the three sonar configurations associated with the various UXO search and ID scenarios. These three configurations are depicted in Fig. 4.

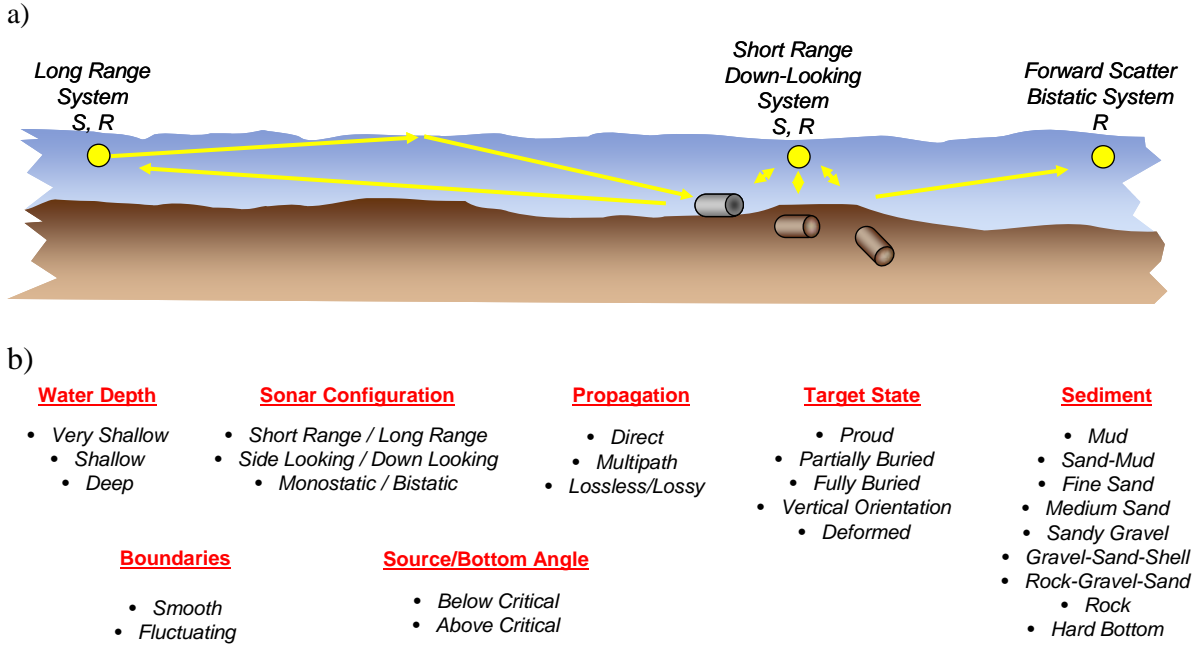


Figure 4 – a) The Three UXO Sonar source/receiver configurations. b) Range of conditions associated with a target strength.

In the long range system (probably mono-static but perhaps bi-static), a source and receivers are located at significant ranges from the targets. The ability to detect at long range allows the possibility of high coverage rates. At long range and in most water depths, the sound would arrive at the target well below the critical angle given by $\theta = \cos^{-1}(C_W/C_S)$ where C_W and C_S are the sound speeds in the water and in the sediment, respectively. At these angles, sufficient sound penetration into the sediment becomes an issue important for buried target detection^{2,14-16}.

The forward scatter system is a special case of the long range bi-static case. Here a bi-static receiver is positioned beyond the target but on a direct line with the incident sound direction. The forward scattered echo¹⁷ is now embedded in the much stronger, overlapping incident sound pulse requiring non-trivial processing to extract the echo with sufficient fidelity. Forward scattering has had some success in the field of ground penetrating radar, and it is of some interest to examine what potential may exist and under what conditions for the underwater UXO problem.

The third sonar configuration is the shorter range, down-looking system. In general such an approach would use both mono-static and bi-static echo responses. Because the downward-directed acoustic energy intercepts the water-sediment interface at angles well above the critical angle, sound penetration into the sediment is not an issue for most bottom types. However, for buried targets since the sound must propagate to the target and the echo back again to the interface, sound absorption could be important, especially at the higher frequencies.

The range of conditions in which any of these sonar systems might have to operate is quite large. These conditions are listed in Fig. 4b.

RESULTS AND ACCOMPLISHMENTS

I. NUMERICAL STUDIES OF FREE-FIELD, PROUD, AND BURIED TARGETS AND THE EFFECTS OF SEDIMENT SURFACE ROUGHNESS

We have carried out numerical studies of backscattering from the 5" rocket UXO near a smooth or rough water-sand interface using EFIT two-dimensional simulation model^{18,19}. The elastodynamic finite integration technique²⁰ (EFIT) code is a time-domain method which uses a time-domain version of a perfectly matched layer (PML) to truncate boundaries. The code is useful for the treatment of pulse propagation in inhomogeneous fluid-elastic environments such as are of interest in the underwater UXO problem. The generality of EFIT allows for the inclusion of stratified bottoms with rough interfaces and volume inhomogeneities such as rocks, shells, and other buried objects. Current code (written by Calvo) has a Cartesian grid and requires computations with and without the target present to isolate scattering. For these numerical studies, the following conditions are applicable: 1) Two-dimensional EFIT numerical models were applied to model scattering at beam incidence; 2) a correction factor of $10\log_{10}(aL^2/2\lambda)$ is added to the 2D target strength to obtain an approximate 3D target strength in order to compare with experimental data; 3) we have neglected attenuation/absorption in the EFIT code (although we plan to include it at a later time); 4) an effective cylinder length (equal to the un-tapered casing length) of 0.3 meters is used.

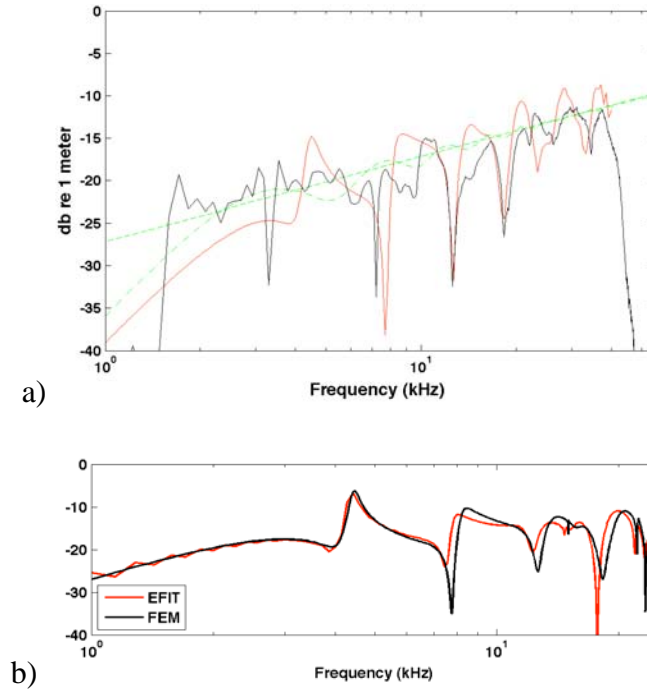


Figure 5 – a) Broadside Target Strength versus Frequency Computed for Infinite Cylindrical Shell with Five Inch Rocket Parameters and 3D Wave Correction Compared to Measurement. Black: measured data; red: COMSOL 2-D FE calculation with 3D wave correction; green-dashed: $10\log_{10}(aL^2/2\lambda)$; green-dashed-dot: wave theory rigid 2D cylinder with finite length 3D wave theory correction. b) Comparison Between the EFIT and Finite Element Broadside Scattering Predictions for Infinite Cylindrical Shell with Five Inch Rocket Parameters and 3D Wave Correction. Target strength in dB: red – EFIT; black- finite element both wave-corrected for 3D.

Shown in Fig. 5a is a comparison of the results of the EFIT 2D model with finite length 3D wave theory correction for an infinite cylindrical shell with 5 inch rocket parameters compared to the measured data for broadside (90°) backscattering. Also shown are the results using 2-D finite element-based model with 3D wave correction. As can be seen, the 3-D corrected EFIT result is in overall agreement with the levels and trends of the measured data. In Fig. 5b is shown the comparison between the EFIT versus finite-element result. As can be seen, the main features are in reasonable agreement, and the discrepancies can likely be eliminated by: 1) modifying EFIT to solve directly for the scattered and not the total field (source effects may cause shifting of the TS with frequency and time-domain methods are like experiments); 2) reducing numerical dispersion or dissipation (although the shell is 13 grid cells thick for EFIT); and 3) using a non-uniform grid instead of a constant step size Cartesian grid. In any case, we believe the agreement is sufficient to allow confidence in the following case study results using EFIT.

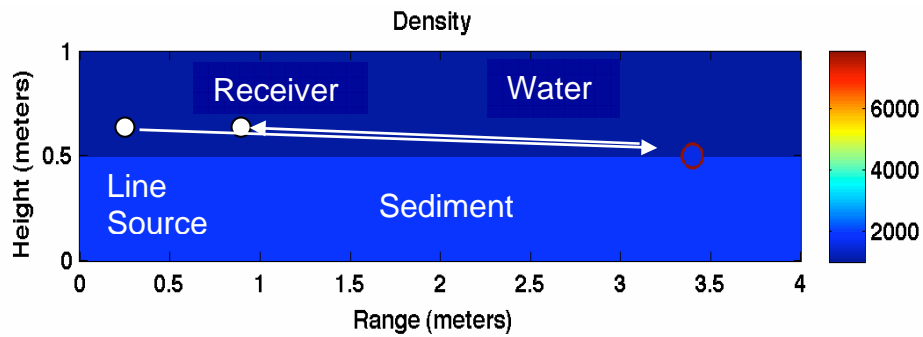


Figure 6 – Scattering Geometry for EFIT Calculations.

Figure 6 shows the geometry for both the EFIT calculations as well as the laboratory measurements. The sediment is assumed non-dispersive with speed 1680 m/s and density 1966 kg/m^3 . The water has sound speed 1482 m/s and density 1000 kg/m^3 . The receiver and source are 10 cm above the sediment, with the former at a 2.01 m range and the latter at a 2.75 m range.

In Fig. 7a we show the comparison between the EFIT simulation and the laboratory measurement⁸ for the free-field target case. Overall, the agreement is reasonably good given the lack of a direct inclusion of scattering and elastic wave interactions that can take place by virtue of the presence of the physical ends of the target

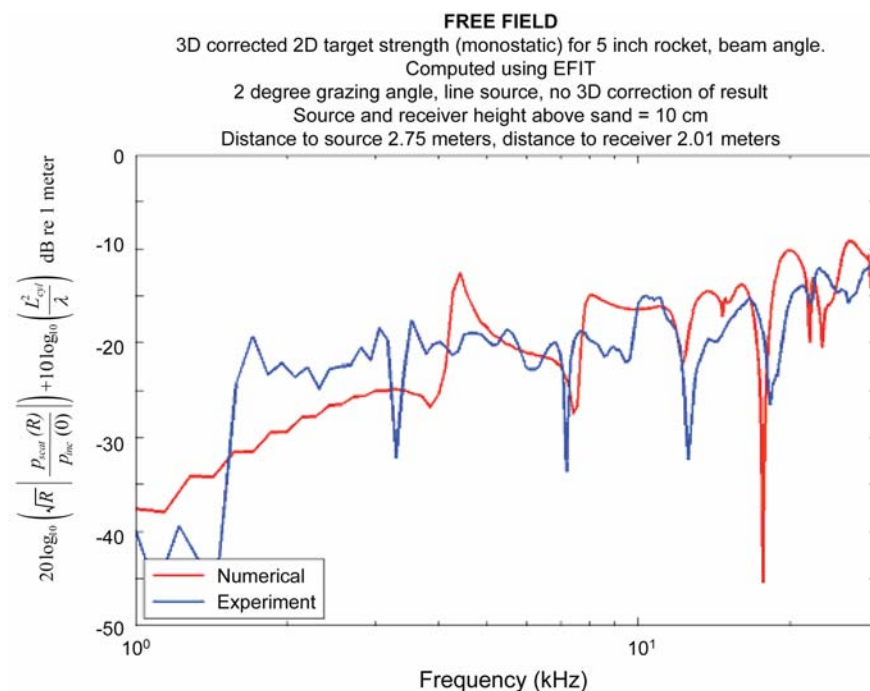


Figure 7a – EFIT Model Result for Infinite Cylindrical Shell with Five Inch Rocket Parameters and 3D Wave Correction Compared to Laboratory Measurement for Free-Field Five-inch Rocket Target.

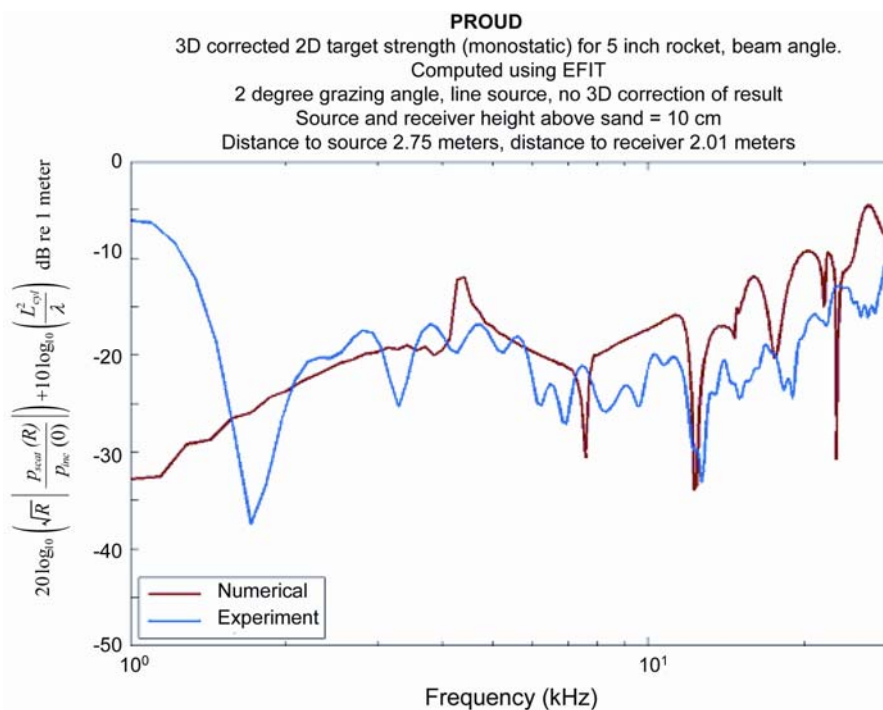


Figure 7b – EFIT Model Result for Proud Infinite Cylindrical Shell with Five Inch Rocket Parameters and 3D Wave Correction Compared to Laboratory Measurement for Proud Five-inch Rocket Target.

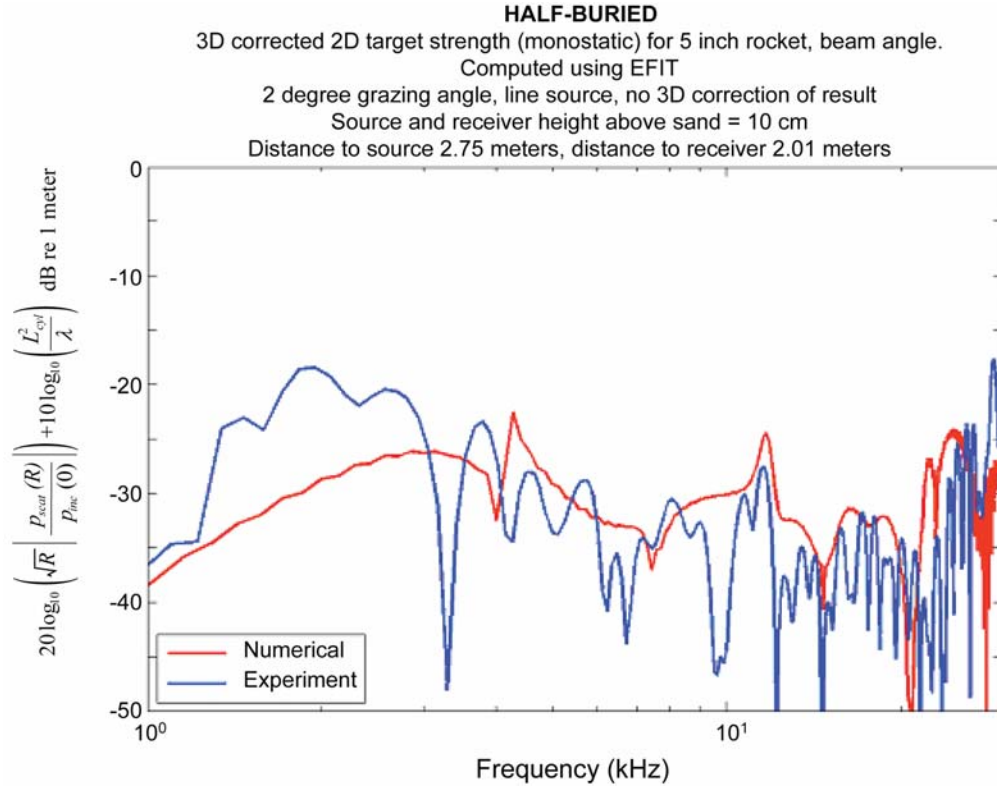


Figure 7c – EFIT Model Result for Half-Buried Infinite Cylindrical Shell with Five Inch Rocket Parameters and 3D Wave Correction Compared to Laboratory Measurement for Half-Buried Five-inch Rocket Target.

In Fig. 7b we show the comparison between the EFIT simulation and the laboratory measurement for the proud target case. Again, the agreement is reasonably good given the lack of a direct inclusion of scattering and elastic wave interactions that can take place by virtue of the presence of the physical ends of the target. The largest disagreement can be seen at around 1 kHz where the measurement shows an anomalously high peak. This peak is not observed in the free-field measurements suggesting that it may be an error in the processing for the measurement.

Next, we show in Fig. 7c the comparison between the EFIT simulation and the laboratory measurement for the half buried target case. Again, the agreement is reasonably good given the lack of a direct inclusion of scattering and elastic wave interactions that can take place by virtue of the presence of the physical ends of the target. We note that the experimentally observed peak in the proud case at the lowest frequencies is not seen in the half-buried case consistent with its absence in the free-field further suggesting that this peak may be related to a processing error in measurement for the proud case.

Finally, we show the calculated beam backscattered target strength for free-field, proud, half buried, and flush buried all plotted together in Fig. 8. It is clear from this figure that for beam backscattering from a cylinder: (1) For a proud target, the impact of the surface of a smooth sediment is minimal compared to the free-field case. In particular, at some frequencies the sediment acts to increase the target strength while at others to decrease it. However, in both cases the changes are relatively small. (2) Burial causes a large decrease in the target strength. Except at the lowest frequencies, even only half burial results in roughly a 10 dB decrease. In the flush burial case, however, there is anywhere from a 15 to 25 dB decrease across the band.

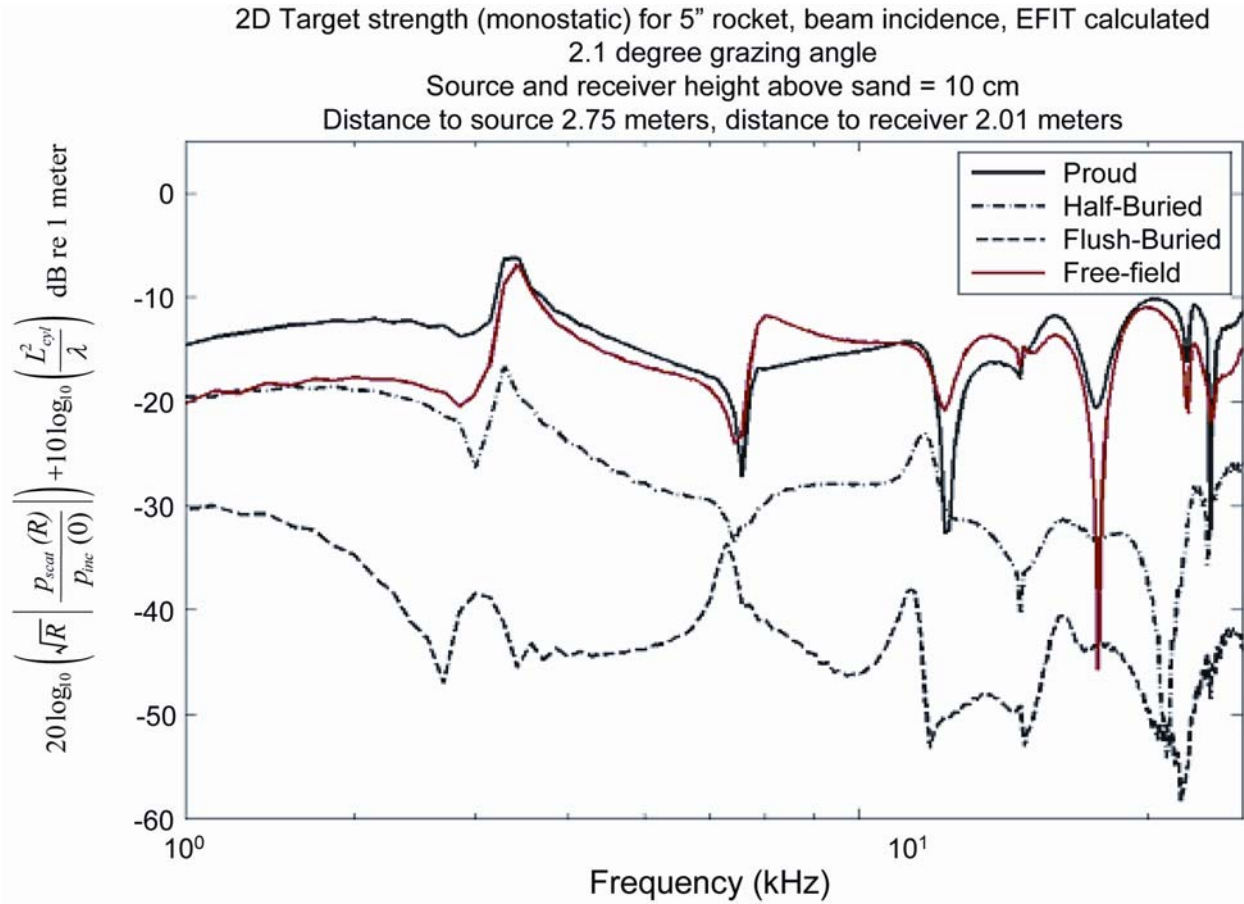


Figure 8. Backscattered Target Strength versus Frequency Calculated Using EFIT Model for Infinite Cylindrical Shell with Five Inch Rocket Parameters and 3D Wave Correction for Geometry Shown in Fig. 6 and Various Burial Conditions.

We have also used the EFIT model to better understand the effects of sediment interface roughness. Two effects due to roughness on which we have focused are (1) the impact of surface roughness on sediment sound penetration and on the subsequent echo from a buried target and (2) the scattering from the rough surface itself which acts as a reverberant field which can mask the returning echo. Other modeling techniques applied to this problem have been either perturbation approaches or high frequency approximations. In contrast, the EFIT method is uniformly valid in all frequency or interface height regimes and can be used to intuit, for example, at what frequency roughness begins to impact bottom penetration and the subsequent echoes.

We first introduce a randomly rough surface height in terms of a power-law spectrum, $W_S(K)$, where $W_S(K) = \eta K^{-\nu}$ if $K_{hp} < |K| < K_{lp}$ and is 0 for all other values of K . Here K is the interface Fourier wavenumber. In the following calculations we take $\nu = 3$, $K_{hp} = 10$ rad/m and $K_{lp} = 31.5$ rad/m. The interface profile is created by Fourier synthesizing the wavenumber spectrum with random (with equal probability) phases chosen between 0 and 2π for each discrete Fourier component. The constant η is chosen such that the RMS height of the interface is 2.5 cm. A Monte-Carlo method was then used to

develop statistics by performing realizations (multiple full calculations in parallel) with typically 15 realizations. Three example realizations are shown in Fig. 9.

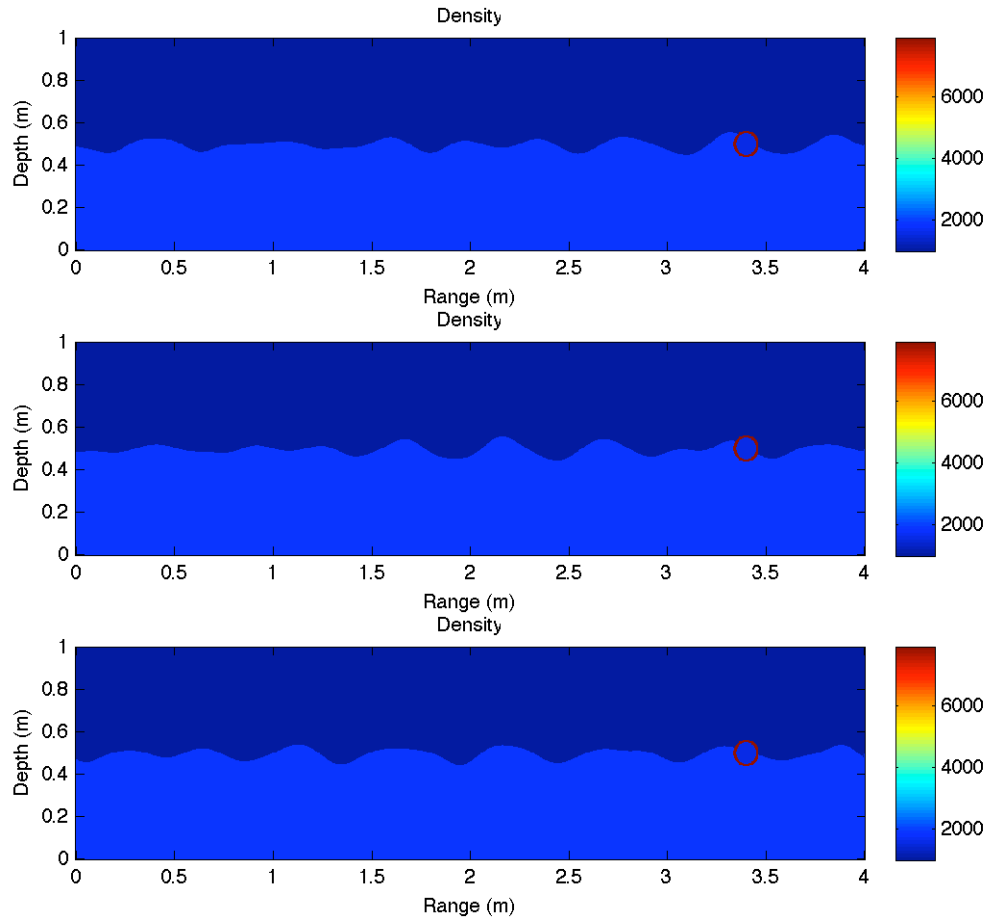


Figure 9 – Example Surface Roughness Realizations.

First, we show the effects of surface roughness with the parameters discussed above on the echo from a flush buried infinite cylinder target insonified at beam. Fig. 10a shows the echo versus frequency and receiver angle for a flat versus rough sediment interface for a 2 degree angle between the source to target direction and the sediment.

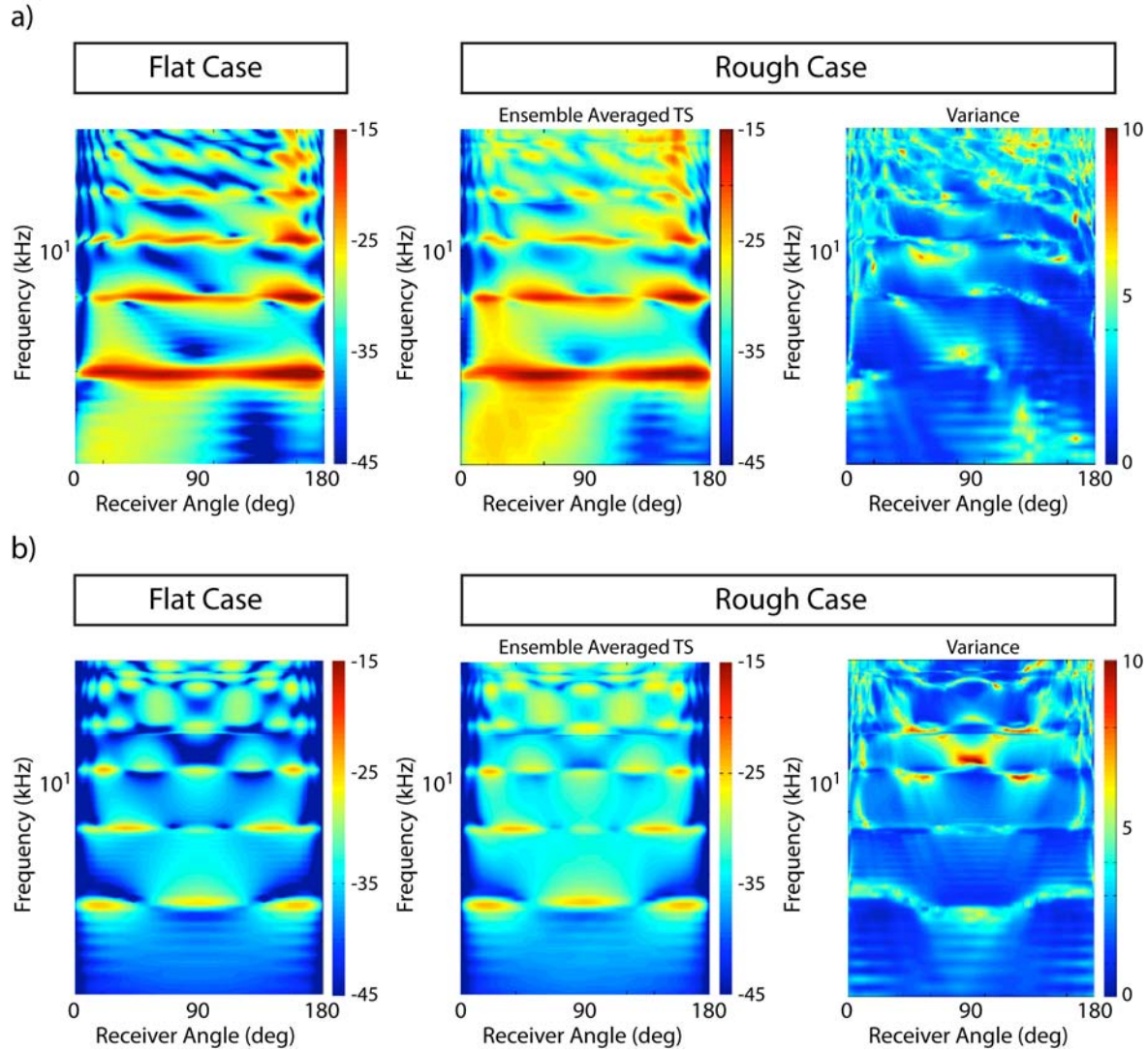


Figure 10 – Target strength versus Frequency and Receiver Angle. Effects of roughness for flush-buried infinite cylinder target with sound incident at beam on the target and a) 2 degrees with respect to the sediment surface; b) 90 degrees with respect to the sediment surface.

Also shown is the variance between the two. As can be seen, on average there is some tendency for the rough surface to fill in the deep nulls and to cause some restructuring of the main frequency-angle features. Generally, but especially at higher frequencies, the variance is largest in the forward direction (180°).

Although the focus of these numerical studies was below critical angle insonification, in Fig. 10b are shown the same displays for the 90 degree source angle (or look-down) case. Here the structure in frequency and angle seems to be more preserved than in the grazing angle case, and the variance in the echo characteristics between flat and rough conditions is for the most part simply a small increase in the background target strength spread throughout frequencies and angles. That the frequency-angle features seem somewhat robust from flat to rough surfaces bodes well for application of the structural acoustic ID technique using the shorter range, look-down sonar configuration.

Next we discuss the time-series simulation results for the backscattered echo which includes contributions from both the sediment interface and a half buried infinite cylinder target insonified at beam by a 2 degree source. The scattered intensity back to the receiver versus time is shown in Fig.11 for an ensemble averaged rough surface compared to that for the flat surface case.

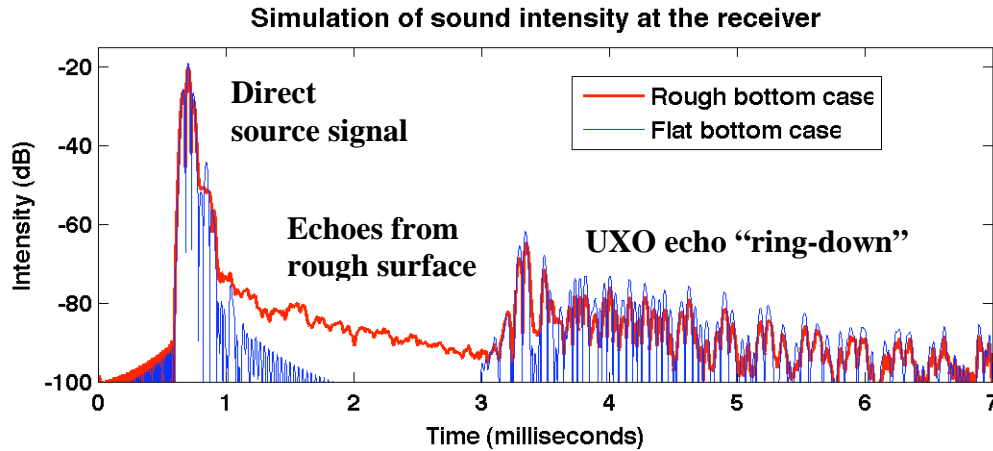


Figure 11 – Ensemble Averaged Reverberation Backscattered Intensity. Time series for the half-buried infinite cylinder and a 2 degree source angle.

In Fig. 12 we show the target (half-buried) echo and the ensemble averaged reverberation backscattered intensity time series for 2°, 28° (critical angle), and 90° source angles. The simulation used a wide-band Ricker source pulse centered at 10 kHz covering a band 2 kHz to 30 kHz. First, we point out two anomalies in the reverberation simulation. First, the small bump just after 4 ms in the 2 degree case is an artifact related to reflection off the PML boundary. Second, the sudden drop in the reverberation seen in the 28 degree and 90 degree cases at long times is caused by the finite domain width used in the calculation (5.7 m). In any case, in the time window of the scattered target response, the reverberation from the rough sediment boundary generally increases as the source angle grows, from grazing conditions at the smallest angle to 90 degrees (having the sound source vertically above the target), and this is not surprising.

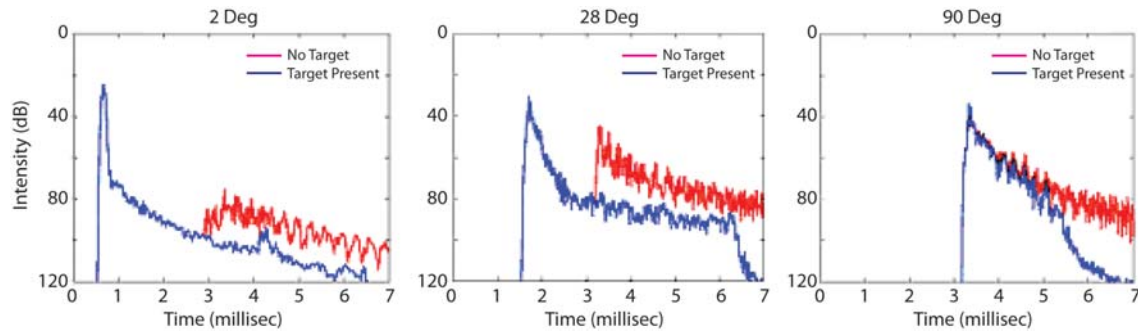


Figure 12 – Ensemble Averaged Target Echo versus Reverberation Backscattered Intensity. The time series are shown for 2°, 28° (critical angle), and 90° source angles. The simulation used a wide-band Ricker source pulse centered at 10 kHz covering a band 2 kHz to 30 kHz.

We make the following general conclusions regarding the effect of the rough sediment surface. At grazing angles (and thus for the more long range configurations), the reverberant background level is only moderately increased. However, there are some probably important changes in the frequency-angle feature structure. At look-down angles, there is a relatively larger increase in the background reverberant level. But there is less change in the frequency-angle structure.

BI-STATIC MEASUREMENTS BELOW THE CRITICAL ANGLE

Generally, experimental studies of scattering from proud or buried targets^{8,21,22,23} have focused on monostatic scattering wherein the source and receiver are co-located. Here we present results^{24,25} related to bistatic scattering and in particular its forward scattered component. We would like to explore whether forward scattering provides some advantage relative to backscattering especially regarding partially buried targets probed below the critical angle of the sediment/water interface.

Many UXO are more or less cylindrical in shape including the particular target whose bistatic target strength (TS) we discuss here. TS is defined in the usual sense⁹ as $10 \log_{10}$ of the ratio of the intensity returned by the target in some direction, at a distance of 1m from its acoustic center, to the incident intensity from a distant source (plane wave). Apart from elastic effects, we can estimate what one would expect for the forward scattered TS of a finite cylinder using the analysis of Ross²⁶ as applied to the radar cross section of a perfectly conducting cylinder. As discussed by Bowman²⁷ for an electromagnetic wave incident normally on an infinite conducting cylinder, the problem reduces to the solution of a scalar wave equation for either horizontal or vertical polarization (parallel or perpendicular to the cylinder axis) of the same form as that for the velocity potential of an acoustic wave with soft or rigid boundary conditions, respectively. For this case, in the short wavelength limit the forward scattered TS depends in large part on the target's projected area with a correction term which takes into account the actual surfaces illuminated by the sound wave.

For the beam incidence (90°) case, Ross²⁶ expression for forward scattering with wavenumber k gives

$$TS = 10 \log \left| \sqrt{\sigma^{PO}(90^\circ)} W \exp\left(\frac{j\pi}{2}\right) + \sqrt{\sigma^{side}} \exp\left(\frac{j3\pi}{4}\right) \right|^2 \quad (2)$$

where $\sigma^{PO}(90^\circ) = 4(aL/\lambda)^2$, $W = W^{hh} \sim 1 + 0.498(ka)^{-2/3} - 0.011(ka)^{-4/3}$ with $\sigma^{side} = 0$ for horizontal polarization, $W = W^{vv} \sim 1 - 0.432(ka)^{-2/3} - 0.214(ka)^{-4/3}$ with $\sigma^{side} = 7/\pi(a^3/\lambda)$ for vertical polarization, λ is the acoustic wavelength, $k = 2\pi/\lambda$, and L and a are the cylinder length and radius. The unity term in the expression for W is the physical optics result while the terms in inverse powers of ka account for the effect of the curvature near the shadow boundary. The last term gives the scattering from the ends.

For 0° incidence, Ross' result gives:

$$TS = 10 \log \left| \left[\sigma^{PO}(0^\circ) \right]^{1/2} \exp\left(\frac{j\pi}{2}\right) + \left[\sigma^{CS}(0^\circ) \right]^{1/2} \exp\left(\frac{j3\pi}{4}\right) \right|^2 \quad (3)$$

where $\sigma^{PO}(0^\circ) = \pi^2(a^2/\lambda)^2$, $\sigma^{CS}(0^\circ) = 0.3(\pi a L)(a/\lambda)$. The first term is the physical optics result and the second term takes into account the contribution from the long, curved surface of the cylinder.

The particular target discussed here is the 5 inch rocket warhead. In last year's report we presented measurements carried out in both free-field and sediment pool facilities with the target placed proud of, and then half buried in, the sediment. In the sediment facility, the source and receiver were 10 cm above the sediment surface; and for source-to-target and receiver-to-target distances used here (2.7 m and 2.0 m), the sound strikes the sediment at an angle much smaller than the critical angle ($\theta_c \sim 27^\circ$).

The bistatic measurement process we employed is similar to that reported in Bucaro et. al.⁸ for the monostatic case which used a nearfield cylindrical source array and a small "point" receiver rotating about the target. The data was collected and processed to recover complex scattering cross-section expressible as TS. The incident acoustic pressure in the form of a broadband pulse, the pool clutter (background) pressure, and the scattered pressure were measured in the following way. First, before positioning the target, the source was excited and the incident pressure measured at the location corresponding to the target center. Second the source was excited and the non-target pressure field measured as a function of θ at each receiver position to be used in the scattering experiment. This measurement contains scattering from pool clutter and, in the forward scattering plane, the incident pressure field. Lastly, the target was inserted and the scattered pressure field as a function of scattering angle θ_s was measured.

The TS was obtained by subtracting measurements made with and without the target. This process removes energy associated with the incident wave for bistatic angles in the forward plane as well as from spurious reflections from the finite-sized pool. With the non-target data file removed from the scattered signal, the range-normalized and incident pressure-normalized parameter $X(f, \theta)$ is formed in terms of the scattered signal, $P_{scat}(f, \theta)$, and the incident field measured at the target center, $P_{inc}(f)$ (see Eq. (1)). Here the r dependent factor removes the effects of range from the pressure ratio term. The scattering data was measured at a range (2 m) which is in the near-field for some target aspects and in the far-field for others. Since bistatic data can be readily projected to the far-field, we performed this projection on all the echo measurements. TS values are then defined and displayed as $10\log_{10}(|X(f, \theta)|^2)$. Measured bistatic TS versus frequency and $\Delta\theta = \theta_s - \theta_i$ is shown in Fig. 13 for $\theta_s = 0^\circ$ and 90° for the free field, proud, and half buried cases. Also shown for comparison is the monostatic TS reported by Bucaro et. al.⁸ versus frequency (2kHz to 25 kHz) and the source angle minus receiver angle. 0° and 90° source angles are on the left and right, respectively. Free-field (upper row), Proud (middle row), and Half-buried (lower row). Monostatic measurements (ref. 8) for the proud target (middle right)

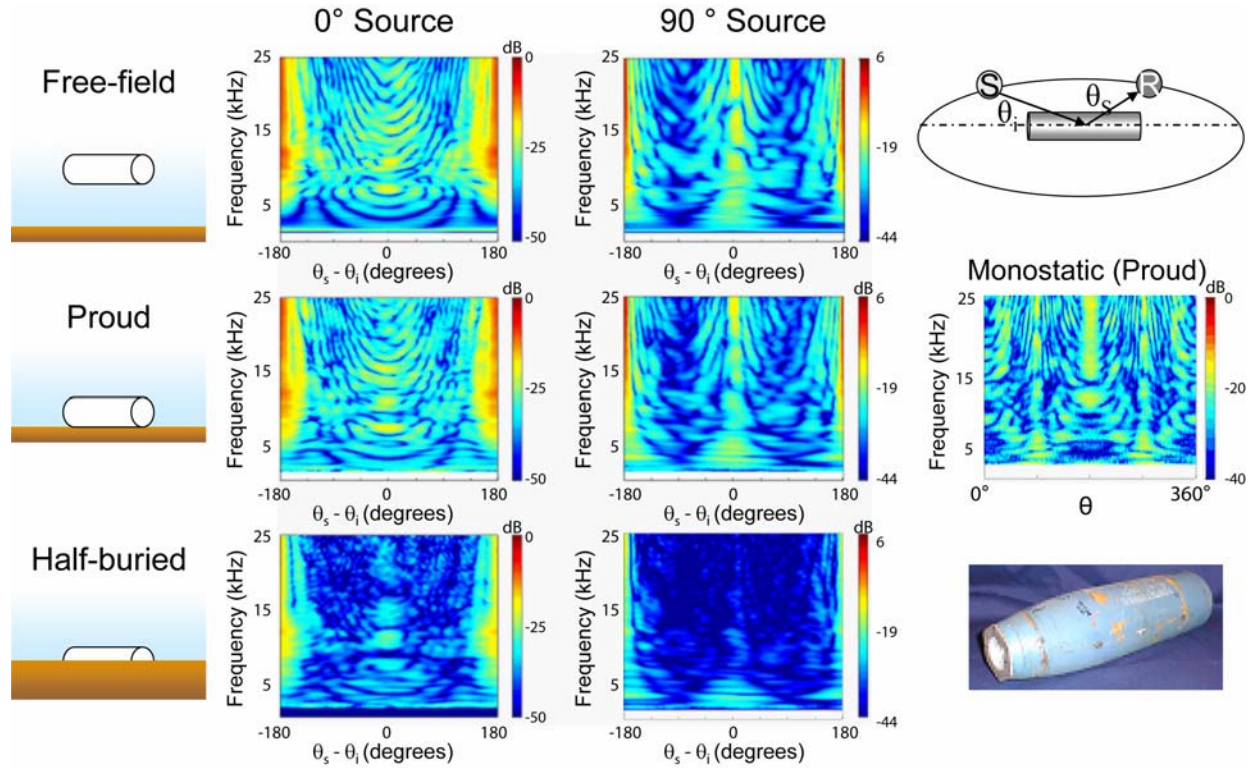


Figure 13 – Bistatic TS measurements for five-inch rocket. Bistatic target strength displayed in dB as a color map measured for the five-inch rocket.

We show in Fig. 14a the result of Eq. (2) compared to the measured free-field data for the beam incidence (90°) case taking the rocket as a circular cylinder of length 18 inches and radius 2.5 inches. As can be seen, the two agree well over almost the entire frequency band. Overall, the data are closer to the rigid result than to the free case which is not surprising given that the target is a relatively thick-walled structure (the cylindrical wall is \sim half inch steel). We note that the sharp peak at the lowest frequencies (which is even more pronounced in the 0° case) is due to a resonance of the air-filled back compartment (the end wall thickness is \sim 0.1 inches) as confirmed by finite element calculations we carried out indicating that at these low frequencies the structure is not totally rigid. As shown in Fig. 14b, for end-on incidence (0°) the agreement is good over most of the band, but Eq. (3) over-predicts TS at the lower frequencies. The analytic result has the same frequency dependence as that computed numerically using a T-matrix approach⁸ for a rigid, hemi-spherically capped cylinder of about the same length for equivalent frequencies up to about 8 kHz. The latter has a TS level about 4dB higher, and this is presumably due to additional scattering from the curved versus flat ends. Why Eq. (3) is higher than the measured result at low frequencies is unclear.

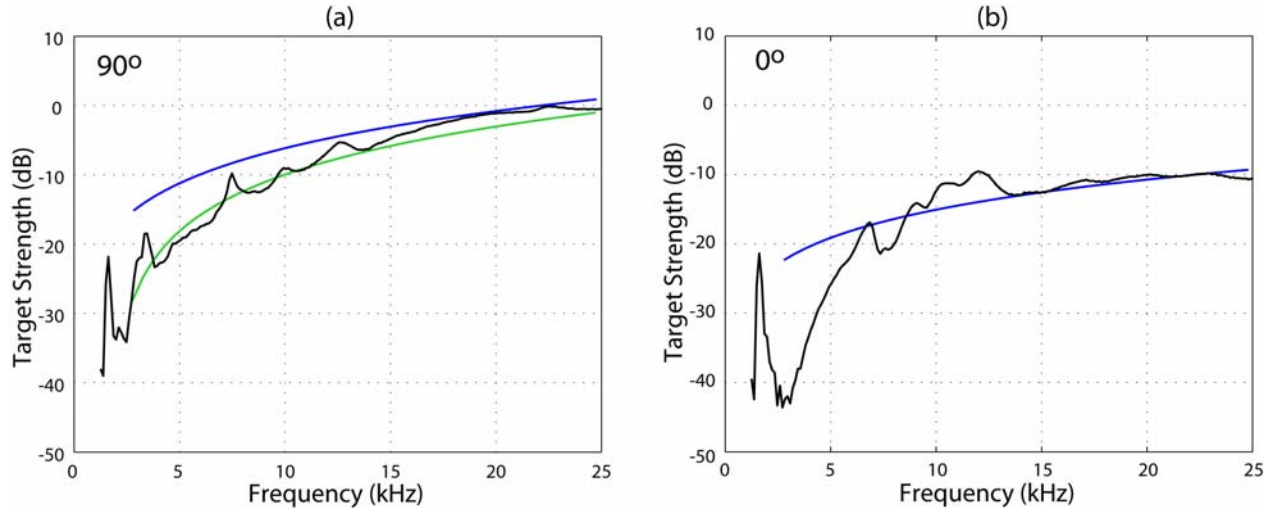


Figure 14 – Measured Forward Scattering TS versus Analytic Model. Measured free-field forward scattered target strength versus frequency in black. (a) 90° source; blue/green soft/rigid boundary condition theory, respectively; (b) 0° source; blue theory.

Consideration of these results and very similar results obtained for the 155 mm shell^{24,25} leads to the following observations. (1) The forward scattered echo has TS levels that are significantly higher than any other return; (2) half burial of the target significantly reduces the backscattered TS levels but not the forward scattered levels; and (3) the leading forward scattering term for both 0° and 90° incidence is $\sigma^{PO}(90^\circ) = 4(aL/\lambda)^2$ and $\sigma^{PO}(0^\circ) = \pi^2(a^2/\lambda)^2$ which are just the projected areas. We therefore expect that the forward scattered TS for other aspects or other targets would be of order the projected areas with a 6 dB per octave increase with frequency.

We conclude that for the $\theta_i < \theta_c$ case, half-buried targets would be difficult to detect in backscattering. The question then becomes: in order to exploit the higher TS levels for the forward scattered echo upon burial, is it possible to extract the forward scattered echo from the strong overlapping incident field *without* having to remove the target as is done in the laboratory measurement?

In the laboratory measurements presented here, we have been able to obtain an accurate measure of the forward scattered TS versus frequency and angle by precise mapping of the incident field (which can be one or more orders of magnitude larger than the scattered pressure) at the receiver locations *prior to target insertion*. This is of course not possible in an actual search in the environment for proud and buried targets. Field approaches which attempt to extract the incident field include for example mode filtering in a water channel²⁶ and apex shifted Radon transforms²⁷ as applied to ground penetrating radar. The former requires long vertical arrays which are not practical for our application. We illustrate here a source estimation technique²⁸ related to the latter²⁷ which uses knowledge of the source location and directivity.

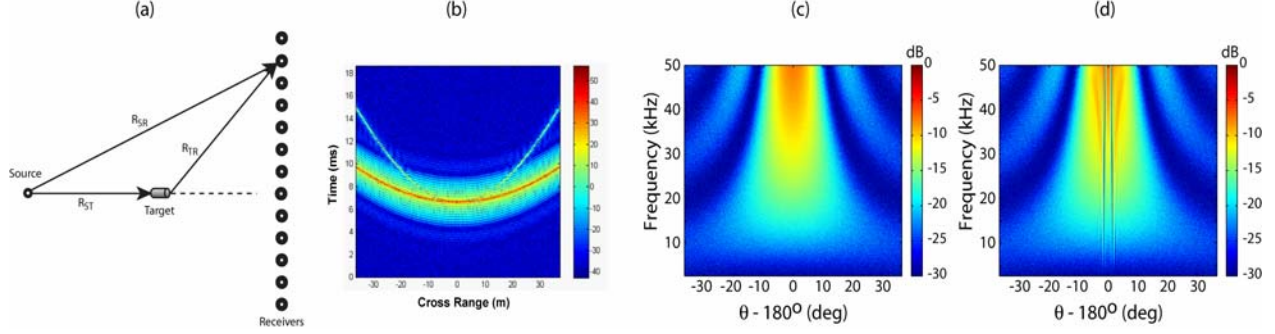


Figure 15. Possible forward Scattering System Geometry, Corresponding Range-Cross Range Plots, and Forward Scattered TS versus Frequency and Angle. (a) Hypothetical long range forward scattering measurement range: R_{ST} , R_{SR} , and R_{TR} are the source to target distance, the distance from the source to a particular receiver, and the distance from the target to a particular receiver, respectively; (b) time-cross range plots in dB for the direct source 150 meters from the center receiver (heavy line) and for the forward scattered signal $\times 30$ with TS given by Eq. 4; (c) scattering TS in dB versus frequency and angle in the forward scattered sector for the scattering response given by Eq. (4); and (d) that extracted from the numerical results shown in (b).

Figure 15a describes a possible source-receiver-target geometry for long range (below critical angle) detection of proud or buried UXO. These receiver positions might be realized, for example, using an autonomous underwater vehicle (AUV) moving in a straight line. The location of the source relative to the i 'th receiver (and therefore the corresponding distance $R_{SR}(i)$ to the i 'th receiver) is assumed known a priori apart from random fluctuations but not R_{ST} or $R_{TR}(i)$, the source to target and target to i 'th receiver distances. In Fig. 15b we show the time versus cross range plots calculated for signals at the various receiver positions due to a broadband (2 kHz to 50 kHz) point source (monopole) at $R_{SR} = 150$ m from the closest receiver together with a forward scattered signal ($\times 30$) from an “unknown” target position (100 m from the source). For the latter we use a TS given by $10\log \sigma^{PO}(0^\circ) = 10\log \pi^2(a^2/\lambda)^2$ (the leading term in Eq. (3) for the 0° source case) since 0° is the aspect with the lowest forward scattered level, and we take that for the 5 inch rocket. The scattering angle dependence (the forward lobe structure) associated with the physical optics area term above is assumed to be that for the far-field diffraction from an aperture of radius a leading to a TS (k, θ) given by

$$TS(k, \theta) = 10\log \left[\frac{a^2}{4} (ka)^2 \frac{\sin^2(ka \sin \theta)}{(ka \sin \theta)^2} \right] \quad (4)$$

where the frequency can be made explicit using $k = 2\pi f/C$ with C the sound speed. We note that the associated scattered pressure we used has an $\exp(j\pi/2)$ phase term (see Eq. (2)). We have also added -30 dB of random Gaussian noise and a random phase term $\exp(j2\pi f C^{-1} \Delta R(i))$ to the i 'th receiver signal with $0 \leq 2\pi f C^{-1} \Delta R(i) \leq 4 \times 10^{-4} \times f$ to simulate random deviations (up to 0.1 m) of the AUV path from a straight line.

As can be seen in Fig. 15b, the source and target scattering signals map into two hyperbolas weakly modulated by the random phase term and noise since both free space Green's functions are of the form $R^{-1} \exp(j2\pi f C^{-1} R)$. Our proposed technique is as follows. (1) There is an angular region (here beyond $\sim \pm 20^\circ$ from forward) with no overlap of source and echo time signals, and here the forward scattered component is directly accessible. (2) In the overlap region, we would like to subtract the “known” source signal at each receiver from the total signal using the appropriate Green's function leaving the desired scattered pressure. However, the source signal is not known precisely due to the unknown random deviations of the AUV (the $\Delta R(i)$) from a straight line. We can, however, estimate each receiver position

deviation by finding the local minimum for the difference between the received signal (the sum of the source, scattered, and noise signals) and an estimate of the source signal based on the known Green's function. Good estimates of the receiver deviations are so obtained because the source signal is much stronger than the other components of the received signal.

Carrying out this procedure on the data in Fig. 15b produces the TS frequency/angle map shown in Fig. 3d compared to that given directly by Eq. (4) in Fig. 15c, both with the added noise. Apart from the obvious artifact (the vertical line structure), the process recovers $TS(f, \theta)$. The line structure corresponds to loci of receiver positions and frequencies where the path difference $R_{ST} + R_{TR} - R_{SR} = \pi/2$, which when added to the $\pi/2$ in the TS phase term (see Eq. (3) leaves the echo with no quadrature component i.e. π out of phase with the source signal. As a consequence, our simple fitting procedure for determining the ΔR incorrectly eliminates the scattered signal at these particular (f, θ) points. Although not shown here, the extracted results and Eq. (4) at exactly 180° agree very well ($\pm 0.3\text{dB}$) over the entire band.

In conclusion, we note that bistatic scattering measurements at vertical angles well below the critical angle made on a 5 inch rocket and a 155 mm shell UXO in the free-field, proud, and half buried in sediment indicate that for these conditions exploitation of forward scattering may provide a detectable signal with levels higher than that for backscattering and one that persists under partial burial. We illustrate for a point source in an infinite medium a technique that might be employed in a relatively simple environment to extract the forward scattered component from the much stronger incident field. Work is underway to develop more sophisticated approaches and to demonstrate them in more complex environments

MEASUREMENTS IN ST. ANDREW'S BAY

In the previous year¹³, scattering measurements were carried out on several proud UXO targets in St. Andrew's Bay where the water depths were on the order of 30 feet. This past year, the data associated with one of the targets, the 155mm shell, was analyzed with reference to measurements made in the sediment pool facility at much shorter ranges. The objective was to understand the differences observed for target scattering in these two environments.

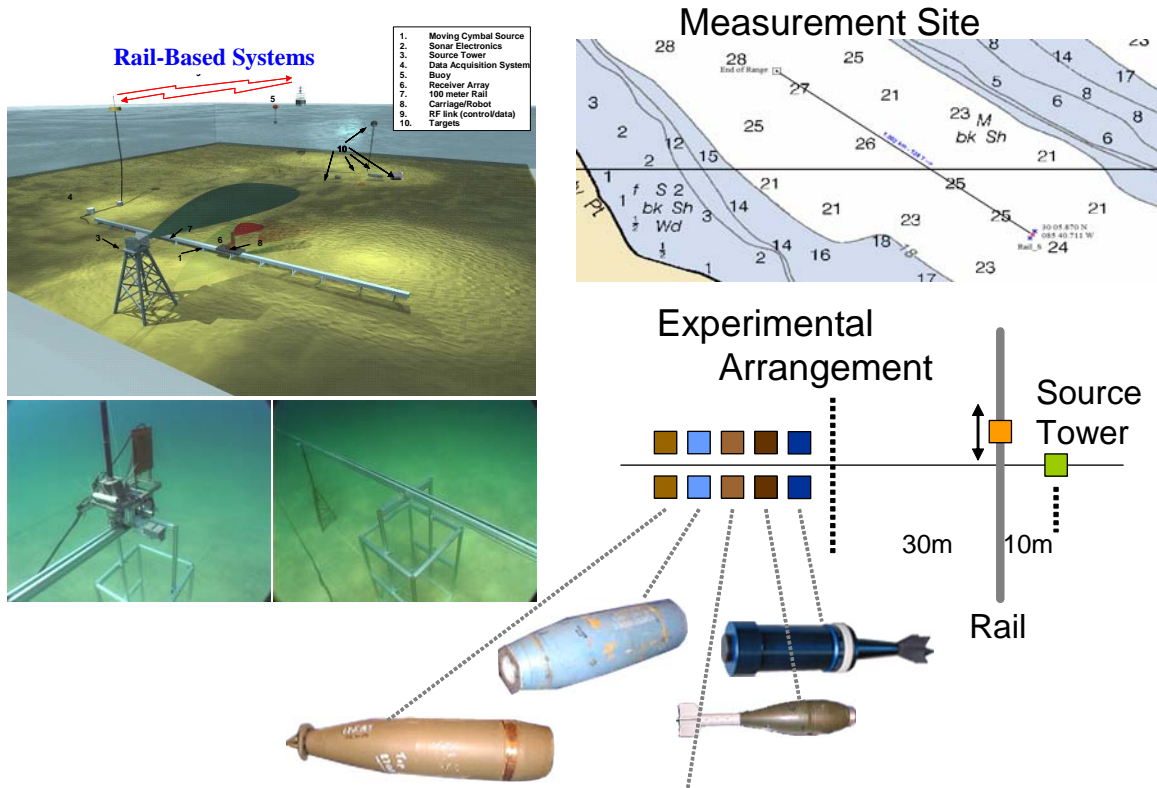


Figure 16 – Measurement Details at St. Andrew's Bay. Upper right: Measurement site and water depths; lower right: UXO targets and their positions and the locations of the source and rail based sensor system; upper left: drawing of the source and rail system with both a moving source and receiver.

The Bay measurements utilized the NRL rail-based system and geometric layout shown in Fig. 16. The two main components are 1) a 30 meter long horizontal rail-based robotic scanner used to collect bistatic scattering data over a limited angular aperture and 2) a two meter long vertical sediment property scanner. The rail-based system is used in conjunction with a fixed impulsive broadband projector mounted to a tower 10 meters up range from the rail as shown in the figure. The different targets were positioned at various distances beyond the 30m separation line from the rail as depicted in the figure. Computer-controlled measurements were executed with the raw scattering response from the fixed broadband projector collected from discrete receiver positions along the 30 meter rail. As with the laboratory-based systems, the data is post processed to extract the broadband scattering cross-sections from the area surveyed by the rail out to 100 meters with $\sim 0.5 - 1$ meter spatial resolution. The sediment property scanner is used to extract the sediment acoustic properties at the rail measurement sites (e.g., sound speed and attenuation vs. frequency and depth).

The measurements were made at the St. Andrews Bay site located in the area also shown in Fig. 16. For the measurements, divers were used to deploy the source tower, the 30 m rail, the UXO targets, and the supporting equipment and cables for the system. Cables were pulled along the bottom to the support vessel named Mr. Offshore anchored in a two point mooring 190 m from the source tower. A military van was used to support all the top-side data acquisition and data processing equipment. The support vessel was placed in a "quiet" state during data acquisition, which required the use of an onboard generator that is vibration isolated from the ship hull. These have become standard operating conditions

for NRL measurements using Mr. Offshore. A plan view of the experimental arrangement is shown in Fig. 16. As can be seen, the targets are placed at positions starting 30 meters from the rail, and although not indicated, the upper row of targets are aligned with their front facing the source (0°) and the lower row with their long side facing the source (90°).

In the measurement exercises at St. Andrew's Bay, bistatic measurements were collected over a limited range of scattering angles determined by the geometry of the rail-based measurement system. For either incident source direction, the bistatic angle range was about $\pm 27^\circ$ about the source direction.

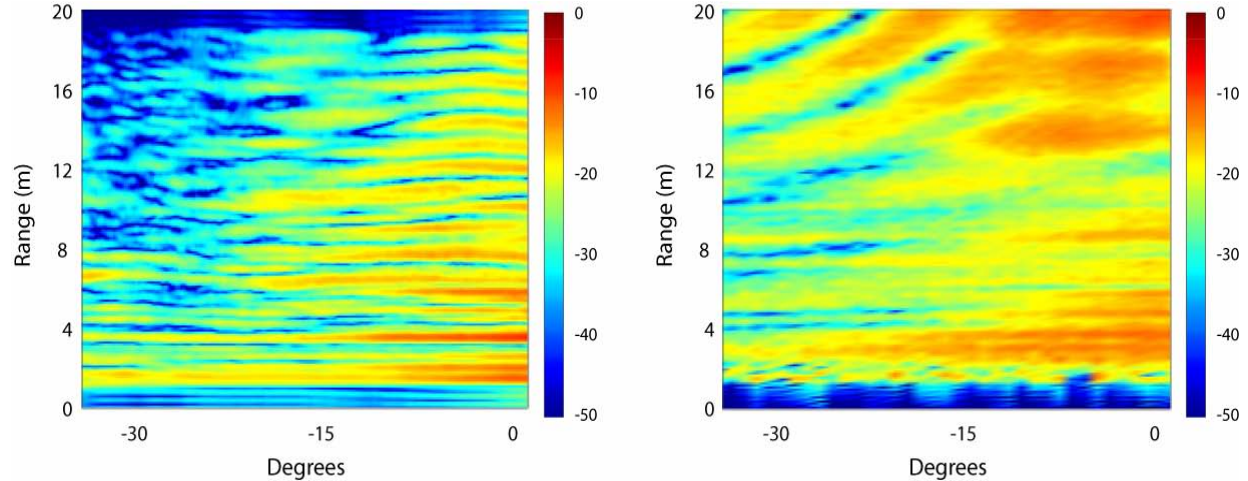


Figure 17 – Measured Target Strength. Magnitude of the bistatic target strength for 0° incidence coded in color versus frequency and scattering angle as measured in the Bay (left) and in the sediment pool (right) for the proud 155 mm shell.

As reported last year¹³ the results for the 155 mm shell 90° incidence case are shown in Fig. 17 together with a comparison to that obtained over the same angular range for the measurements made in the laboratory sediment pool. As can be seen, the overall target strength levels are comparable. However, the frequency-angle patterns are different. Most noticeable is (1) the increased modulation with frequency of the directly backscattered echo for the Bay result, and (2) the lack of the strong bands for the Bay result in the higher frequency/scattering angle region as seen in the pool result. These bands are the modulation in the backscattered beam highlight caused by the finite target length. The frequency/angle shapes of these bands are determined by simple phase matching to the waterborne wave. In Fig. 18 we show line plots of the near backscattered response versus frequency for the 155 mm target. These plots show that at least for the backscattered case, the overall frequency trends are similar.

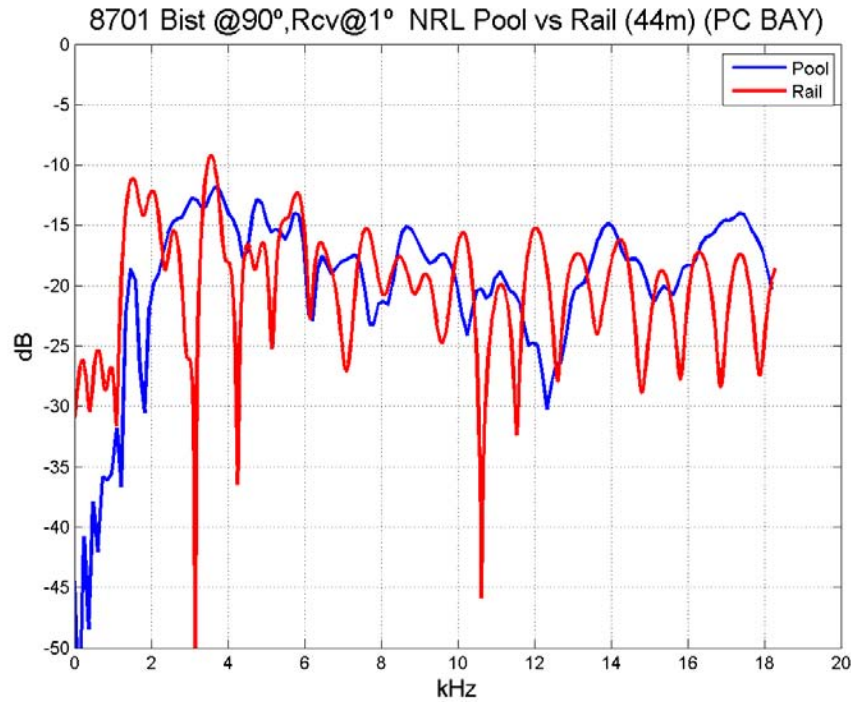


Figure 18 – Measured Target Strength. Magnitude of the bistatic target strength for 0° incidence coded in color map versus frequency and scattering angle as measured in the Bay (left) and in the sediment pool (right) for the proud155mm shell.

The differences observed between the very short range sediment pool measurements and the measurements in the bay are most likely due to one or more of the following conditions: (1) sediment properties; (2) geometric uncertainties; and (3) acoustic propagation. We believe that the largest effect by far relates to the last item, and we have considered this effect in some detail.

In particular, we have used the Range-dependent Acoustic Model (RAM) model developed at NRL by Michael Collins^{29,30}. This model is based on a user-selected multiple-term Padé approximation of the parabolic equation (PE) operator. Because this solution allows range steps much greater than the acoustic wavelength and does not require fine vertical gridding, RAM is a very fast research model.

As an illustrative example³¹, we illustrate both the use of the RAM code and the impact of acoustic multi-path propagation in Fig. 19. Here the previously measured monostatic free-field scattered echo versus frequency and aspect angle for the 155 mm shell is projected using the RAM code to a 78 m range in a 30 foot water column with the properties associated with the measurement area of St. Andrew's Bay. The predicted target echo at that range is shown in the upper right of the figure. Also shown are the time pressure signals we have measured in the fluid and the sediment at 78 m using an array of sensors and what the RAM model would predict for this environment. Each of these consists of a number of signals with different arrival times which are associated with the many propagation paths created by the multiple surface and bottom reflections. Some of these are illustrated in Fig. 20 along with the specific correspondence of a particular ray path with the appropriate time arrival.

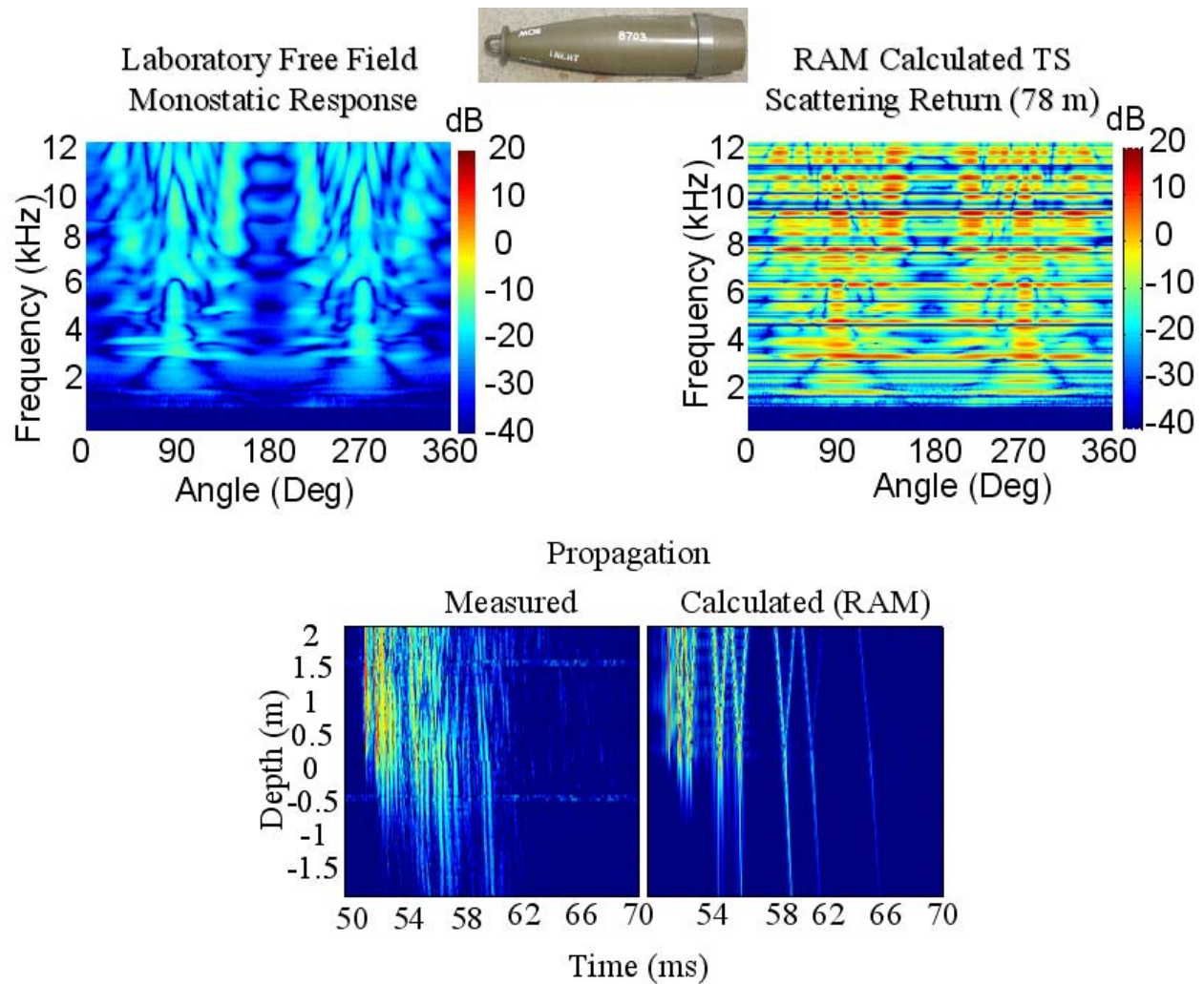


Figure 19 – Simulated Effect of Propagation on the Monostatic TS. Upper left: Measured monostatic free-field target strength versus angle and frequency for the 155mm shell shown in the upper photograph; lower: the measured and simulated (using RAM) acoustic pressure in the water and sediment versus time at the receiver for the St. Andrew's Bay site.

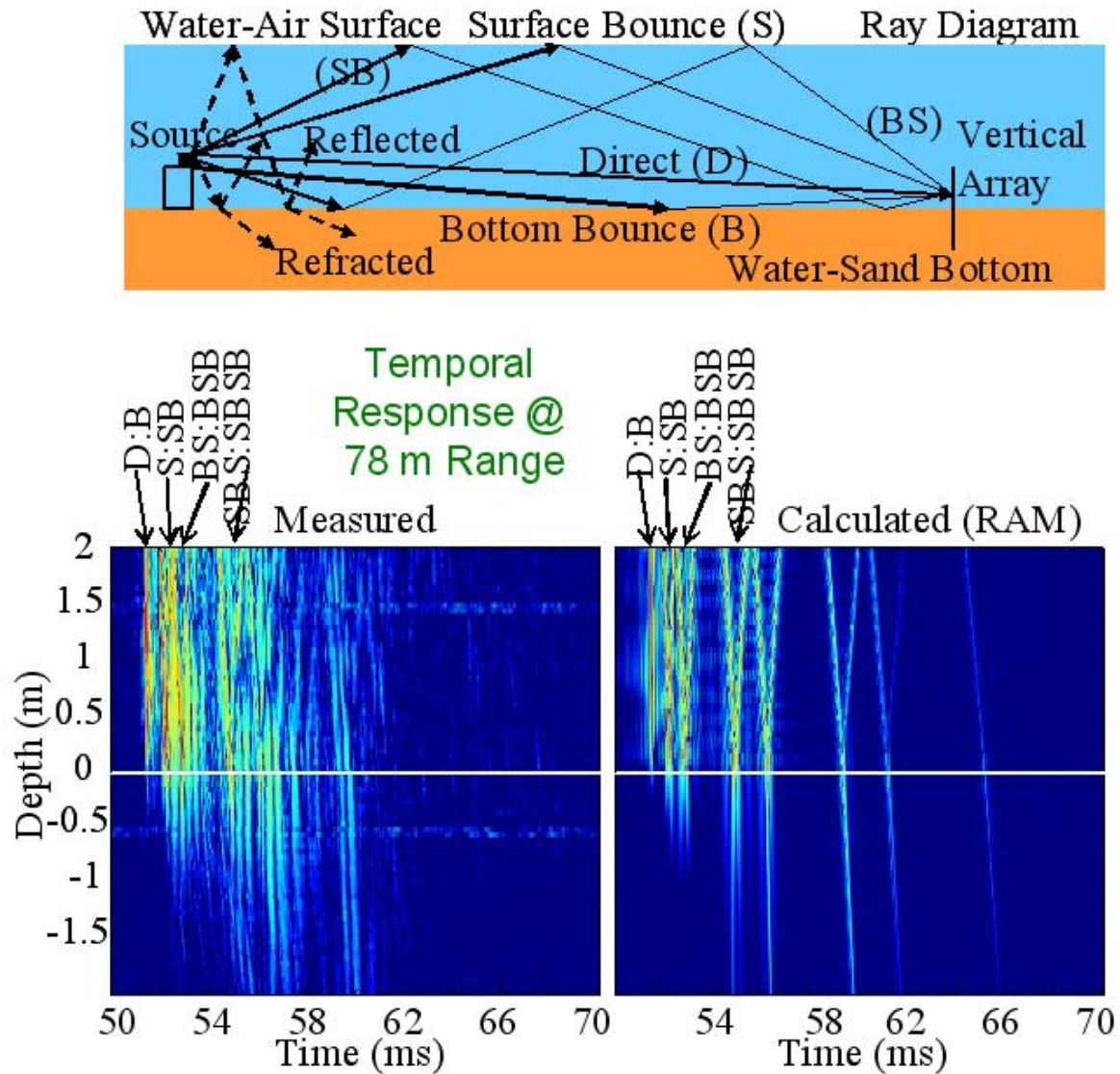


Figure 20 – The Major Rays which Account for the Acoustic Propagation in the Water Column and Sediment. Upper: The important rays from the source to the receiver array; lower: the measured and simulated (using RAM) acoustic pressure in the water and sediment versus time at the receiver for the St. Andrew's Bay site with some of the ray arrival times identified with arrows.

Having demonstrated the use of the RAM code and the effects of multi-path propagation, we now attempt to relate the measured target strength for the 155 mm shell made in the laboratory at short range (2 meters) and which contains only direct path rays to that measured in St Andrew's Bay at a range of 42 m and having significant multi-path propagation. Specifically, we used the RAM code and the free-field measured target strength to predict what would be measured in the Bay, and the results are shown in Fig. 21. As can be seen, this introduction of the effects of multi-path propagation go a long way in producing the frequency-angle patterns actually measured at the longer ranges in the Bay. The remaining differences could be related to several factors. First, the sediment surface, assumed in our RAM projection to be flat, is actually not perfectly so. Second, there is some uncertainty regarding positioning of the target orientation and the source alignment (each of these are on the order of $(\pm 5^\circ)$).

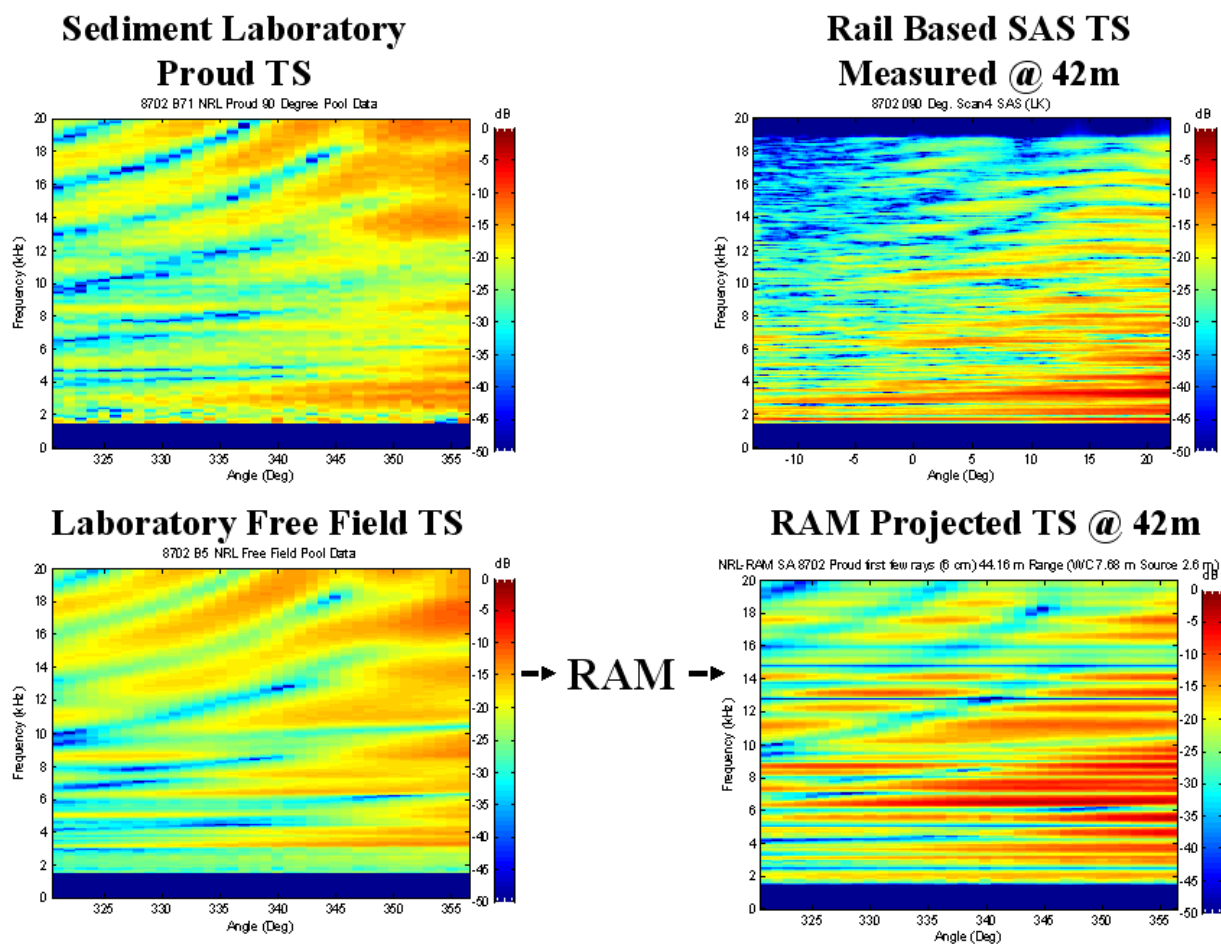


Figure 21. Target Strength versus Frequency and Aspect Measured in St. Andrew's Bay Compared to That Simulated Using RAM and the Laboratory Measured Free-Field TS. In the Bay results, the stationary source and moving receiver are 42 and 52 meters, respectively, from the 155mm shell target.

CONCLUDING REMARKS

The fifth year of the program will focus on the collection of additional at-sea data bases in the structural acoustics frequency band at the Panama City off-shore site and complementary data in the sediment pool facility. The objective here is to more fully characterizing targets and clutter *as they would present themselves in real-world environments*. The focus of the effort will be to understand what features are important for determining whether detections in a real-world environment are or are not associated with a UXO.

REFERENCES AND LINKS

1. B. H. Houston, J.A. Bucaro, T. Yoder, L. Kraus, and J. Tressler, J. Fernandez, T. Montgomery, T. Howarth, "Broadband low frequency sonar for non-imaging based identification," IEEE Oceans 2002.
2. H. J. Simpson and B. H. Houston, "Laboratory measurements of sound scattering from a buried sphere above and below the critical angle," J. Acous. Soc. Am. 113, 39-42 (2003).
3. P. Runkle, L. Carin, L. Couchman, T. Yoder, and J. Bucaro, "Multi-aspect identification of submerged elastic targets via wave-based matching pursuits and hidden Markov models," J. Acous. Soc. Am., vol. 106, pp. 605–616, Aug. 1999.
4. P. Runkle, L. Carin, L. Couchman, T.J. Yoder, and J.A. Bucaro, "Multi-aspect target identification with wave-based matching pursuits and continuous hidden Markov models," IEEE Trans. Pattern Analysis and Machine Intelligence, vol. 21, pp. 1371–1378, Dec. 1999.
5. B. H. Houston, "Structural Acoustic Laboratories at NRL in Washington, D.C.," J. Acoust. Soc. Am. 92(4), October 1992.
6. H.J. Simpson, E.C. Porse, B.H. Houston, L.A. Kraus, A.R. Berdoz, P.A. Frank, and S.W. Liskey, "Very low frequency scattering experiments from proud targets in a littoral environment using a 55 meter rail," J. Acoust. Soc. Am. Suppl. 114 (2003).
7. J. A. Bucaro, B.H. Houston, M. Saniga, H. Nelson, T. Yoder and L.Kraus, and L. Carin, "Wide area detection and identification of underwater UXO using structural acoustic sensors," 1st Annual SERDP Report, December 1, 2006.
8. J.A. Bucaro, B.H. Houston, M. Saniga, L.R. Dragonette, T. Yoder, S. Dey, L. Kraus, and L. Carin, "Broadband acoustic scattering measurements of underwater unexploded ordnance (UXO)," J. Acous. Soc. Am. 123, 738-746 (2008).
9. R. Urick, *Principles of Underwater Sound*, 3rd ed. (McGraw-Hill, New York, NY, 1983), p 291.
10. J.A. Bucaro, B.H. Houston, M. Saniga, A. Sarkissian, H. Nelson, T. Yoder, L. Kraus, and L. Carin, "Wide area detection and identification of underwater UXO using structural acoustic sensors – 2nd annual SERDP Report," December 1, 2007.
11. M. Tipping, "Sparse Bayesian learning and the relevance vector machine," Journal of Machine Learning Research, vol. 1, pp. 211-244, 2001.
12. Xuejun Liao, Hui Li, and Balaji Krishnapuram, "An M-ary KMP classifier for multi-aspect target classification," Proceedings of IEEE International Conference on Acoustics, Speech, and Signal Processing (ICASSP), 2, 61-64 (2004).
13. J. A. Bucaro, B.H. Houston, H. Simpson, L. Kraus, T. Yoder, M. Saniga, A. Sarkissian, and L. Carin, "Wide area detection and identification of underwater UXO using structural acoustic sensors," 3rd annual SERDP report," January 2009.

14. H. J. Simpson and B. H. Houston, "Synthetic array measurements of acoustical waves propagating into a water-saturated sandy bottom for a smooth and roughened interface," *J. Acoust. Soc. Am.*, 107, 2329-2337 (2000).
15. H. J. Simpson, B. H. Houston, S. W. Liskey, P. A. Frank, A. R. Berdoz, and C. K. Fredrickson. "At-sea measurements of sound penetration measurements into sediments using a buried vertical synthetic array," *J. Acous. Soc. Am.* 114, 1281-1290 (2003).
16. H. J. Simpson, C. K. Frederickson, E. C. Porse, B. H. Houston, L. A. Kraus, S. W. Liskey, A. R. Berdoz, P. A. Frank, and S. Stanic, "Measurements of sound propagation in a littoral environment using a vertical synthetic array," *J. Acoust. Soc. Am.* 121, 85-97 (2007).
17. Angie Sarkissian, Charles F. Gaumond, and Louis R. Dragonette, "T-matrix implementation of forward scattering from rigid structures," *J. Acoust. Soc. Am.* 94, 3448-3453 (1993).
18. David C. Calvo, Brian H. Houston, Joseph A. Bucaro, Larry Kraus, Harry J. Simpson, Angie Sarkissian, "Using sound to detect unexploded ordnance (UXO) with variable burial depth and seafloor roughness," October 26, 2009 158th ASA Meeting, San Antonio, TX.
19. David Calvo, Brian Houston, Joseph Bucaro, Larry Kraus, Harry Simpson, Angie Sarkissian, "Scattering by unexploded ordnance (UXO) with variable burial depth and seafloor roughness: a parametric study," October 26, 2009 158th ASA Meeting, San Antonio, TX.
20. D.C. Calvo, K.E. Rudd, M. Zampolli, W.M. Sanders, and L.D. Bibee, "Simulation of acoustic scattering from an aluminum cylinder near a rough interface using the elastodynamic finite integration technique," accepted for publication in *Wave Motion*.
21. Harry J. Simpson, Brian H. Houston, and Raymond Lim, "Laboratory measurements of sound scattering from a buried sphere above and below the critical angle," *J. Acoustic. Soc. Am.* 113, 39-42 (2003).
22. J.L. Lopes, C.L. Nesbit, R. Lim, D. Tang, K.L. Williams, and E.I. Thorsos, "Shallow grazing angle sonar detection of targets buried under a rippled sand interface," *Proceedings of Oceans 2002*, Biloxi, MS, Oct. 28-Nov.1 (2002).
23. A. Tesei, J.A. Fawcett, and R. Lim, "Physics-based detection of man-made elastic objects buried in high-density-clutter areas of saturated sediments," *Appl. Acoust.* 69, 422-437 (2008).
24. J.A. Bucaro, H. Simpson, L. Kraus, L.R. Dragonette, T. Yoder, and B.H. Houston "Bistatic scattering from submerged unexploded ordnance lying on a sediment," *J. Acous. Soc. Am.* 126, 2315-2323 (2009).
25. Joseph A. Bucaro, Brian H. Houston, Larry Kraus, Harry J. Simpson, David C. Calvo, and Louis Dragonette, "Bistatic scattering from underwater unexploded ordnance and the impact of burial," *J. Acoust. Soc. Am.* 125, 2733 (2009).
26. R. A. Ross, "Forward scattering from a finite, circular cylinder," *Progress in Electromagnetics Research C*, 2, 207-215 (2008).
27. J.J. Bowman, T.B.A. Senior, and P.L.E. Uslenghi, *Electromagnetic And Acoustic Scattering by Simple Shapes*, 89-91, Hemisphere Publishing Corporation, New York (1987).

28. J.A. Bucaro, B.H. Houston, H. Simpson, L.R. Dragonette, L. Kraus, and T. Yoder, "Exploiting forward scattering for detecting submerged proud/half-buried unexploded ordnance," J. Acous. Soc. Am. 126, EL171-EL176 (2009).
29. M.D. Collins, "Generalization of the split-step Pade," J. Acoust. Soc. Am. 96, 382-385 (1994).
30. M.D. Collins, R. J. Cederberg, D.B. King, and S.A. Chin-Bing, "Comparison of algorithms for solving parabolic wave equations," J. Acoust. Soc. Am. 100, 178-182 (1996)
31. Harry J. Simpson, Brian H. Houston, Mike L. Saniga, Joseph A. Bucaro, Alain R. Berdoz, and Larry Kraus, "The broadband in-water structural acoustics of unexploded ordnance: tank comparisons with at-sea rail measurements," J. Acoust. Soc. Am. 125, 2733 (2009).

ACKNOWLEDGMENT

This research was supported wholly by the U.S. Department of Defense, through the Strategic Environmental Research and Development Program (SERDP).

APPENDIX

Supporting Data: NA

List of Technical Publications:

- H. J. Simpson, C. K. Frederickson, E. C. Porse, B. H. Houston, L. A. Kraus, S. W. Liskey, A. R. Berdoz, P. A. Frank, and S. Stanic, "Measurements of sound propagation in a littoral environment using a vertical synthetic array," J. Acoust. Soc. Am. 121, 85-97 (2007).
- J.A. Bucaro, B.H. Houston, M. Saniga, L.R. Dragonette, T. Yoder, S. Dey, L. Kraus, and L. Carin, "Broadband acoustic scattering measurements of underwater unexploded ordnance (UXO)," J. Acous. Soc. Am. 123, 738-746 (2008).
- J.A. Bucaro and B.H. Houston, "Sonar systems for prosecuting underwater UXO," SERDP Partners Symposium Workshop, Washington, D.C.(2008).
- David C. Calvo, Brian H. Houston, Joseph A. Bucaro, Larry Kraus, Harry J. Simpson, Angie Sarkissian, "Using sound to detect unexploded ordnance (UXO) with variable burial depth and seafloor roughness," October 26, 2009 158th ASA Meeting, San Antonio, TX.
- David Calvo, Brian Houston, Joseph Bucaro, Larry Kraus, Harry Simpson, Angie Sarkissian, "Scattering by unexploded ordnance (UXO) with variable burial depth and seafloor roughness: a parametric study," October 26, 2009 158th ASA Meeting, San Antonio, TX.
- David C. Calvo, Brian H. Houston, Joseph A. Bucaro, Larry Kraus, Harry J. Simpson, Angie Sarkissian, "Using sound to detect unexploded ordnance (UXO) with variable burial depth and seafloor roughness," October 26, 2009 158th ASA Meeting, San Antonio, TX.

J.A. Bucaro, H. Simpson, L. Kraus, L.R. Dragonette, T. Yoder, and B.H. Houston, "Bistatic scattering from submerged unexploded ordnance lying on a sediment," J. Acous. Soc. Am. 126, 2315-2323 (2009).

J.A. Bucaro, B.H. Houston, H. Simpson, L.R. Dragonette, L. Kraus, and T. Yoder, "Exploiting forward scattering for detecting submerged proud/half-buried unexploded ordnance," J. Acous. Soc. Am. 126, EL171-EL176 (2009).

Joseph A. Bucaro, Brian H. Houston, Larry Kraus, Harry J. Simpson, David C. Calvo, and Louis Dragonette, "Bistatic scattering from underwater unexploded ordnance and the impact of burial," J. Acoust. Soc. Am. 125, 2733 (2009).

Saikat Dey, Angie Sarkissian, Eris S. Mestreau, Brian H. Houston, and Larry Kraus, "Three-dimensional structural-acoustics modeling and its validation for free-field and littoral environments," J. Acoust. Soc. Am. 125, 2702 (2009).

Harry J. Simpson, Brian H. Houston, Mike L. Saniga, Joseph A. Bucaro, Alain R. Berdoz, and Larry Kraus, "The broadband in-water structural acoustics of unexploded ordinance: tank comparisons with at-sea rail measurements," J. Acoust. Soc. Am. 125, 2733 (2009).

Other Technical material: NA